

(VPF), is the best known angiogenic stimulus increasing the vascular permeability of microvessels to circulating macromolecules.¹⁶ This VPF activity is correlated with various vascular pathophysiologicals.³⁴ In contrast, endothelial permeability is not directly affected by bFGF and PDGF, or inhibited by angiopoietin-1, despite their prominent angiogenic activities.^{35,36} Our data show that the effect of RANKL on endothelial permeability is comparable to that of VEGF. Because RANKL does not increase VEGF expression in ECs,¹³ RANKL-induced endothelial permeabilization and angiogenesis appear to be exerted by a direct action on ECs, independent of VEGF. Note that injection of RANKL, like VEGF, into the vitreous cavity causes breakdown of the blood-retinal barrier formed by tight junctions between the retinal vascular endothelial cells, even though the mode of action of RANKL on the retinal vasculature is unknown.

It is interesting that the effects of RANKL on ECs are so similar to those of VEGF. VEGF was originally isolated from the vasculature and was shown to play essential roles in vascular physiology during embryonic development, as well as in the evolution of various diseases of adult vasculature. It has been found that VEGF is also capable of directly enhancing osteoclastic bone resorption and promoting the survival of mature osteoclasts.¹⁷ Conversely, although RANKL was discovered as a factor active in bone remodeling, its role in vascular disease is increasingly recognized.³⁸ For example, inhibition of RANKL with OPG or RANK fusion proteins or RANKL antibodies reduced chronic inflammatory disorders and malignant tumors in animal models, in addition to bone loss caused by osteoporosis.³⁸ Our current and previous findings that RANKL promotes vascular permeabilization, angiogenesis,¹³ and proinflammatory activation provide further evidence of the adverse effects of RANKL on adult vasculature.²⁹

Our data also demonstrate the prominent roles of eNOS in RANKL-induced angiogenesis and vascular permeability *in vitro* and *in vivo*. Many angiogenic factors, but not all, use NO as mediator in their angiogenic effects. Treatment of ECs with RANKL increased NO production, together with increased eNOS activity (Figure 3A-B). Blockage of NO release prevented RANKL-induced EC migration and capillary-like network formation *in vitro*, as well as sprouting of ECs from rat aorta (Figure 5; Figure S3). Both the mouse Matrigel plug assay and the cornea micropocket assay revealed that RANKL-induced neovascularization was substantially impaired in eNOS KO animals (Figure 6; Figure S4). Thus, it is clear that NO generated from eNOS is required for angiogenic responses to RANKL. The signaling mechanism involved in vascular permeabilization is complex and involves a wide array of factors that affect cell-cell junctions, cell-matrix interaction, and cytoskeletal organization. Involvement of protein kinase C (PKC) and Rho-mediated signaling pathways has been demonstrated in the endothelial permeability induced by various stimuli.³⁹ NO also seems important in mediating vascular permeability, but this is context dependent. In ischemia-reperfusion injury models, NO has been shown to maintain vessel integrity.¹⁵ However, it increased vascular permeability in tumors and in chronic inflammation.³⁵ Our present data indicate that NO plays an important role in RANKL-induced vascular permeability because vascular leakage in the skin of mice and in the retina induced by RANKL was significantly reduced in eNOS KO mice, and these *in vivo* findings were confirmed by measuring permeability and VE-cadherin junction in cultured endothelial cells. However, RANKL-induced permeability was not completely blocked by inhibiting NO production, pointing to the contribution of other signaling components such as PKC, which is activated in ECs by RANKL.²⁹

RANKL causes NO production by ECs via PI3K/Akt-dependent eNOS activation (Figure 4A-D). Although eNOS is constitutively expressed in ECs, its activity can be modulated by variation in its level of expression or by reversible phosphorylation on Ser1177.²⁵ Treatment of ECs with RANKL did not alter the levels of eNOS mRNA and protein (Figure 3C). However, it led to phosphorylation of eNOS at Ser1177, a major phosphorylation site for Akt, and this was blocked by a dominant-negative form of Akt. Moreover, blockage of either PI3K or Akt resulted in a significant reduction in NO production in response to RANKL. Recently, we demonstrated the involvement of Src and PLC pathway in RANKL-induced angiogenesis.¹³ However, the Src inhibitor PPI had no effect on RANKL-induced eNOS activation, indicating that Src is not upstream of the Akt/eNOS pathway by RANKL. Our data also point to a predominant role of TRAF6 in the RANKL-induced NO production. Previous studies in nonendothelial cells have shown that TRAF adaptor proteins such as TRAF2, TRAF5, and TRAF6 can associate with the cytoplasmic tail of RANK and activate various intracellular signaling pathways.²⁸ We have recently demonstrated that TRAF2 and TRAF6 play an important role in RANKL-induced NF- κ B activation in endothelial cells, which leads to increased endothelial CAM expression and EC-leukocyte interactions.²⁹ Surprisingly, a dominant-negative form of TRAF6 but not of TRAF2 inhibited NO production and phosphorylation of Akt and eNOS. Because PI3K mediates Akt phosphorylation, TRAF6 probably links the membrane receptor RANK to PI3K in ECs. Therefore, these results suggest a multifaceted role of TRAF6 in the RANK-mediated angiogenic and inflammatory signaling pathways in ECs.

In summary, the present study provides the first evidence that RANKL increases endothelial permeability in addition to stimulating angiogenesis as previously shown, and it reveals that these effects are dependent on endothelium-derived NO. These findings suggest that elevated RANKL levels in the vascular area may lead directly to endothelial activation and may make an important contribution to the occurrence of angiogenesis-dependent inflammatory vascular diseases such as atherosclerosis.

Acknowledgments

This work was supported by Korea Biotech R&D Group of MoST (Ministry of Science and Technology) (research grant M10416130002-04N1613-00210), the Korea Research Foundation of Korean Government (Ministry of Education and Human Resources Development [MOEHRD]) (grant KRF-2003-C00054), Molecular Cellular Biodiscovery Research Group of MoST (grant 2004-01587), and Vascular System Research Center grant from KOSEF.

Authorship

Contribution: J.-K.M. and Y.-G.K. designed the research; J.-K.M., Y.-L.C., J.-H.C., Y.K., and J.H.K. performed the research; Y.-G.K. and J.R. contributed material; J.-K.M., Y.-G.K., and Y.S.Y. collected data; J.-K.M., Y.-G.K., N.M., Y.-M.K., and G.T.O. analyzed data; and J.-K.M. and Y.-G.K. wrote the paper.

Conflict-of-interest disclosure: The authors declare no competing financial interests.

Correspondence: Young-Guen Kwon, Department of Biochemistry, College of Sciences, Yonsei University, Seoul, 120-749, Republic of Korea; e-mail: ygwon@yonsei.ac.kr.

Not for distribution: this preliminary material is embargoed until publication.

References

1. Folkman J. Angiogenesis in cancer, vascular, rheumatoid and other disease. *Nat Med*. 1995;1:27-31.
2. Moulton KS, Heller E, Konecny MA, Flynn E, Palinski W, Folkman J. Angiogenesis inhibitors endostatin or TNP-470 reduce intimal neovascularization and plaque growth in apolipoprotein E-deficient mice. *Circulation*. 1999;99:1726-1732.
3. Walsh MC, Choi Y. Biology of the TRANCE axis. *Cytokine Growth Factor Rev*. 2003;14:251-263.
4. Sattler AM, Schoppet M, Schaefer JR, Hofbauer LC. Novel aspects on RANK ligand and osteoprotegerin in osteoporosis and vascular disease. *Calcif Tissue Int*. 2004;74:103-106.
5. Bucay N, Sarosi I, Dunstan C, et al. Osteoprotegerin-deficient mice develop early onset osteoporosis and arterial calcification. *Genes Develop*. 1998;12:1260-1268.
6. Min H, Morony S, Sarosi I, et al. Osteoprotegerin reverses osteoporosis by inhibiting endosteal osteoclasts and prevents vascular calcification by blocking a process resembling osteoclastogenesis. *J Exp Med*. 2000;192:463-474.
7. Collin-Osdoby P. Regulation of vascular calcification by osteoclast regulatory factors RANKL and osteoprotegerin. *Circ Res*. 2004;95:1046-1057.
8. Sandberg WJ, Yndestad A, Oie E, et al. Enhanced T-cell expression of RANK ligand in acute coronary syndrome: possible role in plaque destabilization. *Arterioscler Thromb Vasc Biol*. 2006;26:857-863.
9. Bennett BJ, Scatena M, Kirk EA, et al. Osteoprotegerin inactivation accelerates advanced atherosclerotic lesion progression and calcification in older ApoE-/- mice. *Arterioscler Thromb Vasc Biol*. 2006;26:2117-2124.
10. Collin-Osdoby P, Rothe L, Anderson F, Nelson M, Maloney W, Osdoby P. Receptor activator of NF- κ B and osteoprotegerin expression by human microvascular endothelial cells, regulation by inflammatory cytokines, and role in human osteoclastogenesis. *J Biol Chem*. 2001;276:20659-20672.
11. Kartsogiannis V, Zhou H, Horwood NJ, et al. Localization of RANKL (receptor activator of NF- κ B ligand) mRNA and protein in skeletal and extraskelatal tissues. *Bone*. 1999;25:525-534.
12. Min JK, Kim YM, Kim JM, et al. Vascular endothelial growth factor up-regulates expression of receptor activator of NF- κ B (RANK) in endothelial cells. Concomitant increase of angiogenic responses to RANK ligand. *J Biol Chem*. 2003;278:39548-39557.
13. Kim YM, Kim JM, Lee YM, et al. TNF-related activation-induced cytokine (TRANCE) induces angiogenesis through the activation of Src and phospholipase C (PLC) in human endothelial cells. *J Biol Chem*. 2002;277:6799-6805.
14. Rudic RD, Shesely EG, Maeda N, Smithies O, Sogal SS, Sessa WC. Direct evidence for the importance of endothelium-derived nitric oxide in vascular remodeling. *J Clin Invest*. 1998;101:731-736.
15. Murohara T, Asahara T, Silver M, et al. Nitric oxide synthase modulates angiogenesis in response to tissue ischemia. *J Clin Invest*. 1998;101:2567-2578.
16. Fukumura D, Gohongi T, Kadambi A, et al. Pre-dominant role of endothelial nitric oxide synthase in vascular endothelial growth factor-induced angiogenesis and vascular permeability. *Proc Natl Acad Sci U S A*. 2001;98:2604-2609.
17. Jaffe EA, Nachman RL, Becker CG, Minick CR. Culture of human endothelial cells derived from umbilical veins. Identification by morphologic and immunologic criteria. *J Clin Invest*. 1973;52:2745-2756.
18. Wong BR, Rho J, Arron J, et al. TRANCE is a novel ligand of the tumor necrosis factor receptor family that activates c-Jun N-terminal kinase in T cells. *J Biol Chem*. 1997;272:25190-25194.
19. Lee OH, Kim YM, Lee YM, et al. Sphingosine 1-phosphate induces angiogenesis: its angiogenic action and signaling mechanism in human umbilical vein endothelial cells. *Biochem Biophys Res Commun*. 1999;264:743-750.
20. Oura H, Bertoni J, Velasco P, Brown LF, Carmeliet P, Delpire M. A critical role of placental growth factor in the induction of inflammation and edema formation. *Blood*. 2003;101:560-567.
21. Braman RS, Hendrix SA. Nanogram nitrite and nitrate determination in environmental and biological materials by vanadium (III) reduction with chemiluminescence detection. *Anal Chem*. 1989;61:2715-2718.
22. Drabkin DS, Ausin JH. Spectrophotometric constants for common hemoglobin derivatives in human, dog, and rabbit blood. *J Biol Chem*. 1932;98:719-725.
23. Min JK, Lee YM, Kim JM, et al. Hepatocyte growth factor suppresses vascular endothelial growth factor-induced expression of endothelial ICAM-1 and VCAM-1 by inhibiting the nuclear factor- κ B pathway. *Circ Res*. 2005;96:300-307.
24. Bazzoni G, Dejana E. Endothelial cell-to-cell junctions: molecular organization and role in vascular homeostasis. *Physiol Rev*. 2004;84:869-901.
25. Lee MJ, Thangada S, Claffey KP, et al. Vascular endothelial cell adherens junction assembly and morphogenesis induced by sphingosine-1-phosphate. *Cell*. 1999;99:301-312.
26. Shiojima I, Walsh K. Role of Akt signaling in vascular homeostasis and angiogenesis. *Circ Res*. 2002;90:1243-1250.
27. Dimmeler S, Fleming I, Fisslthaler B, Hermann C, Busse R, Zeiher AM. Activation of nitric oxide synthase in endothelial cells by Akt-dependent phosphorylation. *Nature*. 1999;399:601-605.
28. Chung JY, Park YC, Ye H, Wu H. All TRAFs are not created equal: common and distinct molecular mechanisms of TRAF-mediated signal transduction. *J Cell Sci*. 2002;115:679-688.
29. Min JK, Kim YM, Kim SW, et al. TNF-related activation-induced cytokine (TRANCE) enhances leukocyte adhesiveness; induction of ICAM-1 and VCAM-1 via TRAF and PKC-dependent NF- κ B activation in endothelial cells. *J Immunol*. 2005;175:531-540.
30. Glass CK, Witztum JL. Atherosclerosis: the road ahead. *Cell*. 2001;104:503-516.
31. Ross R. Atherosclerosis—an inflammatory disease. *N Engl J Med*. 1999;340:115-126.
32. Crotti T, Smith M, Hirsch R, et al. Receptor activator NF- κ B ligand (RANKL) and osteoprotegerin (OPG) protein expression in periodontitis. *J Periodontol Res*. 2003;38:380-387.
33. Collett GD, Canfield AE. Angiogenesis and pericytes in the initiation of ectopic calcification. *Circ Res*. 2005;96:930-938.
34. Weis SM, Cheresh DA. Pathophysiological consequences of VEGF-induced vascular permeability. *Nature*. 2005;437:497-504.
35. Fukumura D, Yuan F, Endo M, Jain RK. Role of nitric oxide in tumor microcirculation. Blood flow, vascular permeability, and leukocyte-endothelial interactions. *Am J Pathol*. 1997;150:713-725.
36. Thurston G, Rudge JS, Ioffe E, et al. Angiopoietin-1 protects the adult vasculature against plasma leakage. *Nat Med*. 2000;6:460-463.
37. Nakagawa M, Kaneda T, Arakawa T, et al. Vascular endothelial growth factor (VEGF) directly enhances osteoclastic bone resorption and survival of mature osteoclasts. *FEBS Lett*. 2000;473:161-164.
38. Hofbauer LC, Schoppet M. Clinical implications of the osteoprotegerin/RANKL/RANK system for bone and vascular diseases. *JAMA*. 2004;292:490-495.
39. Mehta D, Rahman A, Malik AB. Protein kinase C- α signals rho-guanine nucleotide dissociation inhibitor phosphorylation and rho activation and regulates the endothelial cell barrier function. *J Biol Chem*. 2001;276:22614-22620.

PPARと誘導型シクロオキシゲナーゼの関係

Relationship between PPAR and COX-2



井上 裕康

Hiroyasu INOUE

奈良女子大学生活環境学部食物栄養学科

◎アラキドン酸から生成されるプロスタグランジン(PG)は代表的な生理活性脂質である。15-deoxy- $\Delta^{12,14}$ PG₂は PPAR の内因性リガンド候補として報告され、さまざまな生理作用が見出されている。この分子は種々の蛋白質のシステイン残基に共有結合することにより PPAR γ リガンドとは異なる作用機構が報告されているが、PPAR γ リガンド結合部分に共有結合し、合成リガンドとは異なった作用をもつ可能性も報告された。一方著者らは、PG 産生の律速酵素・誘導型シクロオキシゲナーゼの発現を抑制する天然物質の探索から赤ワインに含まれるポリフェノール・レスベラトロールを見出し、この分子が PPAR α および γ のデュアルアゴニストになることを報告した。アピゲニン(パセリ)、フムロン(ビールホップ)についても同様な性質をもつ。これらの知見は、生活習慣病予防の視点から分子作用機構の解明が期待されるとともに、PPAR がさまざまな生理活性脂質のセンサーとして働いている可能性を示している。



Key Word : プロスタグランジン, PPAR, シクロオキシゲナーゼ, レスベラトロール

シクロオキシゲナーゼ(COX)はプロスタグランジン(PG)産生の律速酵素で、アラキドン酸を基質にして PGH₂を生成する反応を触媒する。非ステロイド性抗炎症薬の作用は COX 活性の阻害による PG 産生抑制に由来する。COX には構成型発現を示す COX-1 と誘導型 COX-2 の 2 種類のアイソザイムが存在する。COX-2 の発現は炎症性刺激で迅速に誘導され、かつグルココルチコイドによって抑制されることから、炎症反応への関与が想定されている。さらに、COX-2 ノックアウトマウスの解析や最近の臨床、疫学調査を含む研究などから、COX-2 が発癌、Alzheimer 病、循環器系疾患にも関与し、さまざまな役割を担っていることがしだいに明らかになってきた¹⁾。

グルココルチコイドや活性型ビタミン D など生理活性をもつ脂溶性物質であり、これらをリガンドとする核内受容体群はその構造上の相同性によってファミリーを形成している。PPAR はこの核内受容体ファミリーに属するリガンド依存性転写因子で、3 種類のサブタイプ α , β (δ), γ が

知られており、それぞれ異なった生理作用に寄与している²⁾。さらに、リガンド存在下で PPAR γ は不安定化するのに対し PPAR α は逆に安定化するとの報告があり、共通のリガンドに対しても異なる働きをもつ可能性がある。PPAR のリガンド結合部位については結晶構造が決定され、ほかの核内受容体に比べ、リガンド結合ポケットが大きいと報告された³⁾。この特徴がさまざまな脂溶性の物質をリガンドとして結合する PPAR の性質に関与しており、一般的なホルモンと受容体の関係とは異なっていると考えられる。PPAR γ の内因性リガンド候補として PGD₂ の代謝産物 15-deoxy- $\Delta^{12,14}$ PG₂ (15d-PGJ₂) が報告された^{4,5)}。また、アラキドン酸をはじめとする脂肪酸やその代謝産物、非ステロイド性抗炎症薬なども PPAR のリガンドとして働く可能性が指摘され、食生活とも密接にかかわる核内受容体であることがわかってきた。

図 1 に COX 経路および、リポキシゲナーゼ経路で PPAR のリガンドとして働く可能性があるも

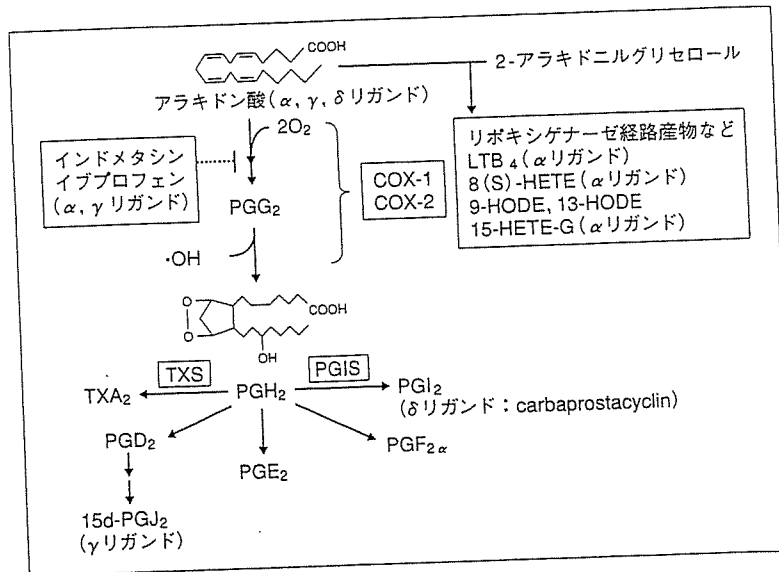


図 1 アラキドン酸カスケードとPPARリガンド

のを示す。注目すべきこととして、PPAR が関与していると考えられる生体内での役割は、前述した COX-2 が関与する役割と重複している点が多い。

マクロファージにおけるPPAR γ による COX-2発現のフィードバック制御

循環器系においては、プロスタサイクリン (PGI₂) とそれに拮抗する作用をもつトロンボキサン (TXA₂) の産生のバランスがホメオスタシスに重要であり、そのバランスの破綻は動脈硬化症をはじめとするさまざまな病態と関連している。PGI₂ はおもに血管内皮細胞で、TXA₂ は血小板や活性化マクロファージで産生されるが、血小板以外の細胞では COX-2 の発現が種々の刺激により誘導され、それぞれの PG 類産生に寄与している。著者らはその視点から、PGI₂ を産生する培養血管内皮細胞と、TXA₂、PGE₂ を産生するマクロファージ系 U937 細胞での COX-2 発現の相違に注目して研究を進めてきた^{6,7)}。

そのなかの研究で、U937 細胞において、COX-2 の発現がデキサメタゾン (DEX) や 15d-PGJ₂ で抑制されること、その抑制効果は血管内皮細胞では認められないことを見出した^{8,9)}。U937 細胞におけるこの抑制効果は、それぞれの受容体であるグルココルチコイド受容体 (GR)、PPAR γ の発現に依存していたが、100 nM DEX では COX-2 の発

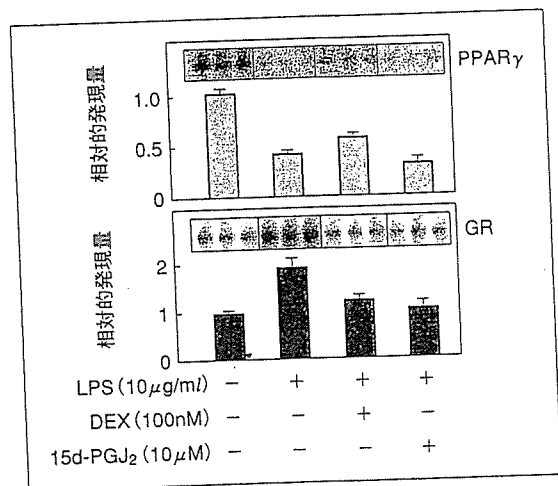


図 2 逆の発現パターンを示す PPAR γ とグルココルチコイド受容体 mRNA⁹⁾

現 が 90% 以上抑制されるのに対し、10 μ M 15d-PGJ₂ では 60% 程度の抑制しか観察されない。GR mRNA の発現はリポポリサッカライド (LPS) 刺激で上行制御されるのに対し PPAR γ は逆に下行制御されること (図 2) から、DEX と 15d-PGJ₂ の COX-2 発現抑制効果の相違は、核内受容体 GR と PPAR γ の発現量に関与していること、さらに GR と PPAR γ の 2 種類の核内受容体は COX-2 の発現に関して異なった役割をもつと考えられる。

つまり LPS 刺激により COX-2 が誘導され、多量の PG が産生された状態 (活性化マクロファ

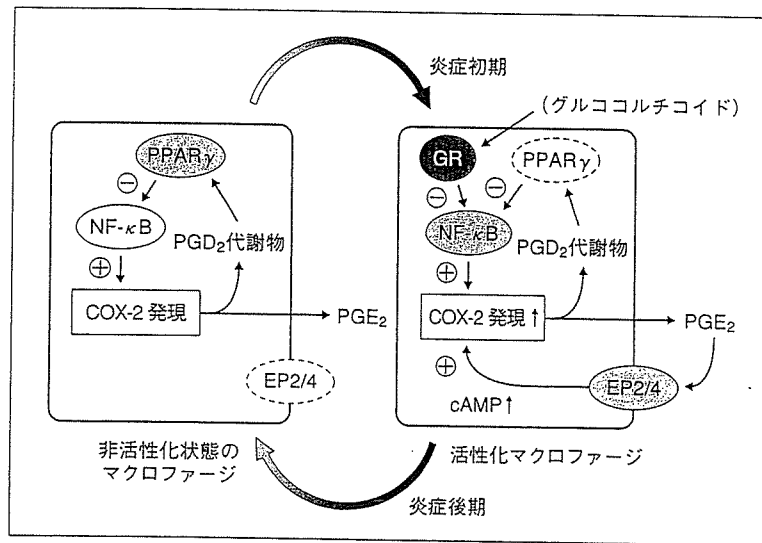


図3 PPAR γ を介するCOX-2発現のフィードバック制御⁹⁾

ジ)において、GRの発現上昇によってDEXに対するCOX-2の発現抑制感受性が上がる。それに対して、PPAR γ はLPS刺激で下行制御されるため15d-PGJ₂に対する感受性は低下する。一方、活性化される前のマクロファージ(応答性マクロファージ)では15d-PGJ₂がCOX-2の発現を抑制していると考えられる。さらに、このような細胞では造血器型PGD合成酵素が発現しており、15d-PGJ₂の前駆体となるPGD₂がCOX-2に依存して産生されることを見出した。これらの知見からマクロファージにおいてはPGD₂代謝産物がPPAR γ のリガンドとして作用することによって負のフィードバック制御を受けることが示唆された(図3)。

一方、活性化状態になりPPAR γ によるフィードバック制御から開放されたCOX-2の発現はPGE₂の産生を促し、それがマクロファージ系細胞で発現する細胞膜型受容体EP2あるいはEP4に働き、細胞内cAMP濃度を上昇させ、COX-2の発現を増強する。このように、時間により異なる種類のPG産生が核内受容体と細胞膜型受容体へ異なる情報を伝達することで、マクロファージにおけるダイナミックなPG産生を可能にしていると考えられる^{9,10)}。

最近COX-2選択的阻害薬投与によって心筋梗塞や脳卒中の危険度が増加することが報告されて

いるが、COX-2の生理的働きには二面性があると考えられる(図4)。それは既述したように、マクロファージ系細胞と血管内皮細胞でCOX-2の発現が異なった制御を受けることから想定されるが、関連する知見として常在性マクロファージではプロスタサイクリン合成酵素とCOX-2が発現していること、応答性マクロファージではCOX-2の発現が抑制されていること、活性化マクロファージではCOX-2発現の増加とともに、トロンボキサン合成酵素の発現が強まることがあげられる¹¹⁾。また、血管内皮細胞において静脈血程度の弱い流れ刺激でCOX-2が誘導され、PGI₂産生に関与していること¹²⁾、さらに強い流れ刺激を与えたりポカリン型PGD₂合成酵素が誘導され¹³⁾、それによって合成されたPGD₂代謝産物(15d-PGJ₂)が細胞保護作用、抗炎症作用、平滑筋増殖抑制作用に関与すると考えられる¹⁴⁾。

15d-PGJ₂の問題点

尿中や培養液中における測定の結果、15d-PGJ₂は内因性リガンドではないとする報告がなされた¹⁵⁾。さらに、15d-PGJ₂は親電子性化合物であることから、さまざまな蛋白質(I κ Bキナーゼ、Nrf2、チオレドキシシン、チオレドキシシン還元酵素、H-ras、プロテアソーム系、c-Junなど)との共有結合を介して作用することが報告されている¹⁶⁾。15d-PGJ₂

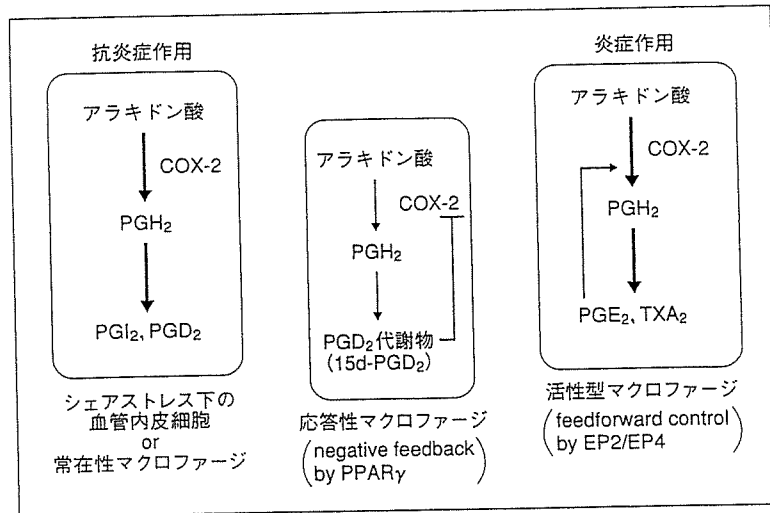


図 4 COX-2の二面性

のさまざまな生理作用を考慮すると、PPAR γ に依存しない、これらの作用機構も重要である。一方で、15d-PGJ₂がPPAR γ のリガンド結合部分に共有結合して働くことが報告された¹⁷⁾。この場合、15d-PGJ₂の13位の炭素にリガンド結合ポケット内のシステイン残基が共有結合(マイケル付加反応)をしており、他の蛋白質で報告されている9位の炭素に蛋白質表面に露出したシステイン残基が共有結合する場合とは異なっていることが指摘されている。さらに、15d-PGJ₂の α,β -不飽和ケトン構造がPPAR γ 活性化に重要であり、この構造をもつ化合物が内因性リガンドとして働くこと、その作用は合成リガンドにおける活性化と異なっていることを報告している¹⁷⁾。魅力的な提案であり、今後の検証が待たれる。

15d-PGJ₂はPGE₂の代謝産物であるPGA₂とともに、以前より抗腫瘍活性、抗ウイルス活性、細胞周期のG₁停止活性が示されている。通常のPGにはG蛋白質共役型の細胞膜型受容体の存在が明らかになっているが、PGJ₂およびPGA₂シリーズのPGには細胞膜型受容体が見出されておらず、核に移行することが知られていた。なおPGA₂をリガンドとする核内受容体としてNR4Aファミリー(Nur77, Nurr1, NOR1)が報告されている¹⁸⁾。また、細胞内でCOXは小胞体と核膜の両方に検出される。したがって、15d-PGJ₂がPPAR γ の内因性リガンドとして働くことはこれらの知見と一貫性を

もつように考えられるが、さらに検討をしていく必要がある。

植物ポリフェノール類

レスベラトロールは赤ワインに含まれる、抗酸化作用をもつフィトアレキシン(抗菌性物質)である。レスベラトロールは、中等度のワイン消費が心血管病、脳卒中、痴呆の危険度と負の相関を示す、いわゆる“フレンチパラドックス”に関与する物質と考えられてきた。著者らは、①レスベラトロールは核内受容体群のうち、PPAR α およびPPAR γ を選択的に活性化すること、②その活性化は血管内皮細胞およびニューロンで認められること、③レスベラトロールおよびPPAR α リガンドを3日間経口投与後に、24時間脳虚血にすると、脳梗塞の体積がコントロールに比べ有意に減少し、脳保護効果が認められること、④その脳保護効果はPPAR α ノックアウトマウスでは認められないことを明らかにした。これらの結果から、レスベラトロールによるPPAR α の活性化は“フレンチパラドックス”を説明する新しい作用機構を提供すると考えている¹⁹⁾。

共同研究のなかで著者らは、レスベラトロールがCOX-2の発現を抑制することを以前に報告しているが²⁰⁾、それ以外の天然物質としてプロポリスに含まれるクリシン²¹⁾、マンゴスチンに含まれる γ -マンゴスチン²²⁾も報告してきた。それ以外の

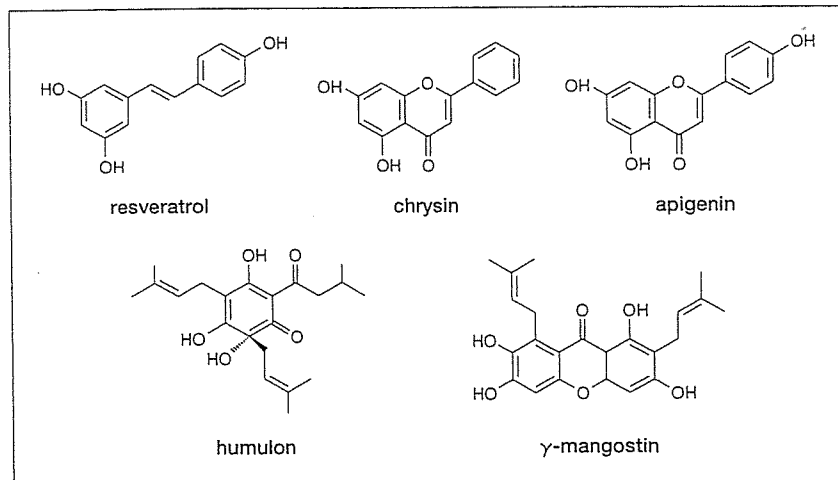


図 5 COX-2の発現を抑制する天然物質

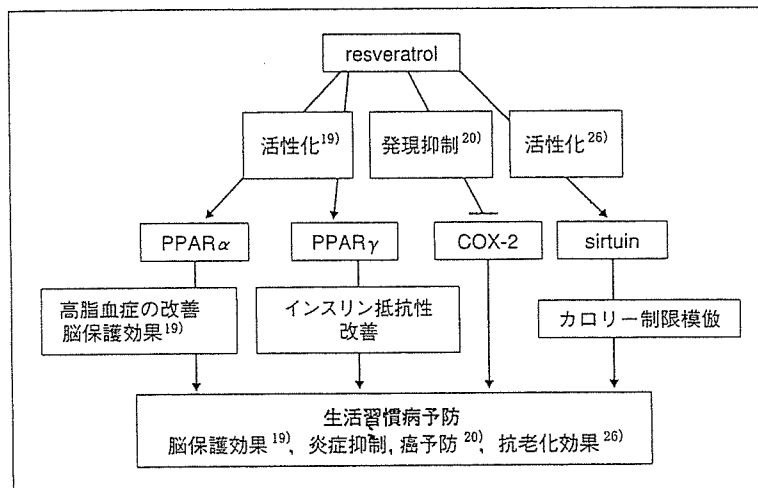


図 6 レスベラトロールのさまざまな作用

天然物質としてパセリに含まれるアピゲニン²³⁾、ピールホップ成分であるフムロン²⁴⁾が報告されている(図5)。興味深いことに、 γ -マンゴスチンを除いて、これらの物質はいずれも PPAR α あるいは γ のアゴニストとしても報告されている^{23,25)}。著者らは現在、さまざまな植物ポリフェノールについて、PPAR 活性化能を指標にして検討を行っており、その構造と PPAR 活性化との関連、COX-2 発現抑制効果との関連を明らかにしていきたいと考えている。これらの研究は食による生活習慣病予防のエビデンスにつながっていくと期待している。

おわりに

以前よりカロリー制限はラットで老化を遅らせ、寿命を延長させることが知られている。そこでカロリー制限の機構を解明し、その効果のみを模倣する薬剤の開発が行われている。そのスクリーニングの結果、興味深いことにレスベラトロールが見出され、酵母の寿命をのばすことが報告された²⁶⁾。その効果は NAD⁺依存性脱アセチル化酵素 Sirtuin ファミリーの活性化に由来すると報告されたが、Sirtuin はさまざまな転写調節に関与しており、核内受容体とも相互作用していると考えられる。最近、DNA チップによる解析で、カ

ロリー制限を行ったネズミと核内受容体 PPAR α のアゴニストを投与したネズミではよく似た遺伝子の発現パターンを示すことが報告され²⁷⁾, 著者らも同様な結果をレスベラトロール投与で得ている(投稿準備中)。しかし一方で, レスベラトロールで活性化される Sirtuin は PPAR γ の活性化を抑制することで, 白色脂肪細胞において脂肪代謝を活性化するという報告もなされた²⁸⁾。この結果は, レスベラトロールが PPAR γ も同時に活性化するという著者らの結果とは一致しない。

現在までの報告を単純に並列にまとめると図6のようになる。注目すべきことに, レスベラトロールに関して, さまざまな *in vivo* の効果を示す論文が多数報告されている^{29,30)}。したがって, PPAR, COX, Sirtuin などのような関係にあるのかを明らかにすることは, 生活習慣病予防の視点から今後の検討されるべき価値があると考えられる。

文献

- 1) 室田誠逸, 山本尚三(編): プロスタグランジン研究の新展開。東京化学同人, 2001, pp.111-141.
- 2) Evans, R. M. et al. : *Nat. Med.*, **10** : 355-361, 2004.
- 3) Xu, M. E. et al. : *Proc. Natl. Acad. Sci. USA*, **98** : 13919-13924, 2001.
- 4) Forman, B. M. et al. : *Cell*, **83** : 803-812, 1995.
- 5) Kliewer, S. A. et al. : *Cell*, **83** : 813-819, 1995.
- 6) Inoue, H. et al. : *FEBS Lett.*, **350** : 51-54, 1994.
- 7) Inoue, H. et al. : *J. Biol. Chem.*, **270** : 24965-24971, 1995.
- 8) Inoue, H. et al. : *Biochem. Biophys. Res. Commun.*, **254** : 292-298, 1998.
- 9) Inoue, H. et al. : *J. Biol. Chem.*, **275** : 28028-28032, 2000.
- 10) 井上裕康: ビタミン, **77** : 449-458, 2003.
- 11) Kuwamoto, S. et al. : *FEBS Lett.*, **409** : 242-246, 1997.
- 12) Inoue, H. et al. : *Arterioscler. Thromb. Vasc. Biol.*, **22** : 1415-1420, 2002.
- 13) Taba, Y. et al. : *Circ. Res.*, **86** : 967-973, 2000.
- 14) Sasaguri, T. and Miwa, Y. : *Curr. Vasc. Pharmacol.*, **2** : 103-114, 2004.
- 15) Bell-Parikh, L. C. et al. : *J. Clin. Invest.*, **112** : 945-955, 2003.
- 16) 柴田貴広, 内田浩二: 生化学, **77** : 1189-1192, 2005.
- 17) Shiraki, T. et al. : *J. Biol. Chem.*, **280** : 14145-14153, 2005.
- 18) Kagaya, S. et al. : *Biol. Pharm. Bull.*, **28** : 1603-1607, 2005.
- 19) Inoue, H. et al. : *Neurosci. Lett.*, **352** : 203-206, 2003.
- 20) Subbaramaiah, K. et al. : *J. Biol. Chem.*, **273** : 21875-21882, 1998.
- 21) Woo, K. J. et al. : *FEBS Lett.*, **579** : 705-711, 2005.
- 22) Nakatani, K. et al. : *Mol. Pharmacol.*, **66** : 667-674, 2004.
- 23) Liang, Y. C. et al. : *FEBS Lett.*, **496** : 12-18, 2001.
- 24) Yamamoto, K. et al. : *FEBS Lett.*, **465** : 103-106, 2000.
- 25) Yajima, H. et al. : *J. Biol. Chem.*, **279** : 33456-33462, 2004.
- 26) Howitz, K. T. et al. : *Nature*, **425** : 191-196, 2003.
- 27) Corton, J. C. et al. : *J. Biol. Chem.*, **279** : 46204-46212, 2004.
- 28) Picard, F. et al. : *Nature*, **429** : 771-776, 2004.
- 29) Lastra, C. A. and Villegas, I. : *Mol. Nutr. Food Res.*, **49** : 405-430, 2005.
- 30) Baur, J. A. and Sinclair, D. A. : *Nat. Rev. Drug Discov.*, **5** : 493-506, 2006.

* * *

Solution Structure of the Cytoplasmic Region of Na⁺/H⁺ Exchanger 1 Complexed with Essential Cofactor Calcineurin B Homologous Protein 1^{*[S]}

Received for publication, April 28, 2006, and in revised form, October 6, 2006. Published, JBC Papers in Press, October 18, 2006, DOI 10.1074/jbc.M604092200

Masaki Mishima[‡], Shigeo Wakabayashi[§], and Chojiro Kojima^{‡1}

From the [‡]Graduate School of Biological Sciences, Nara Institute of Science and Technology, Ikoma, Nara 630-0192, Japan and [§]Department of Molecular Physiology, National Cardiovascular Center Research Institute, Suita, Osaka 565-8565, Japan

Na⁺/H⁺ exchanger 1 (NHE1) regulates intracellular pH, Na⁺ content, and cell volume. Calcineurin B homologous protein 1 (CHP1) serves as an essential cofactor that facilitates NHE1 exchange activity under physiological conditions by direct binding to the cytoplasmic juxtamembrane region of NHE1. Here we describe the solution structure of the cytoplasmic juxtamembrane region of NHE1 complexed with CHP1. The region of NHE1 forms an amphipathic helix, which is induced by CHP1 binding, and CHP1 possesses a large hydrophobic cleft formed by EF-hand helices. The apolar side of the NHE1 helix participates in extensive hydrophobic interactions with the cleft of CHP1. We suggest that helix formation of the cytoplasmic region of NHE1 by CHP1 is a prerequisite for generating the active form of NHE1. The molecular recognition detailed in this study also provides novel insight into the target binding mechanism of EF-hand proteins.

Na⁺/H⁺ exchangers comprise a family of countertransport proteins that catalyze the electroneutral exchange of Na⁺ and H⁺. Nine isoforms of the Na⁺/H⁺ exchanger have been isolated and shown to possess similar membrane topologies consisting of 12 N-terminal membrane-spanning helices and a large C-terminal cytoplasmic region (Fig. 1A). The exchanger isoforms exhibit tissue-specific expression, membrane localization, and kinetic and pharmacological properties (1). They participate in a broad range of physiological processes including the regulation of cell volume, transepithelial transport of electrolytes, cell proliferation, apoptosis, and differentiation.

^{*} This work was supported in part by grants-in-aid for Scientific Research on Priority Area and the 21st Century of Excellence (COE) Program from the Ministry of Education, Culture, Sports, Science and Technology (MEXT), Japan (to M. M. and C. K.), and Grant nano-001 for Research on Advanced Medical Technology from the Ministry of Health, Labor and Welfare of Japan and Grant-in-aid for Priority Areas 13142210 for Scientific Research from the MEXT (to S. W.). The costs of publication of this article were defrayed in part by the payment of page charges. This article must therefore be hereby marked "advertisement" in accordance with 18 U.S.C. Section 1734 solely to indicate this fact.

[‡] The on-line version of this article (available at <http://www.jbc.org>) contains supplemental Table S1 and Figs. S2 and S3.

The atomic coordinates and structure factors (code 2E30) have been deposited in the Protein Data Bank, Research Collaboratory for Structural Bioinformatics, Rutgers University, New Brunswick, NJ (<http://www.rcsb.org/>).

¹ To whom correspondence should be addressed: Graduate School of Biological Sciences, Nara Institute of Science and Technology, 8916-5 Takayama, Ikoma, Nara 630-0192, Japan. Tel.: 81-743-72-5571; Fax: 81-743-72-5579; E-mail: kojima@bs.naist.jp.

Isoforms NHE1–5, localized at the plasma membrane, are primarily involved in the regulation of intracellular pH (pH_i)² and Na⁺ concentration (1).

Of them, the ubiquitously expressed isoform NHE1 is the best studied mammalian Na⁺/H⁺ exchanger. The activity is controlled by various extrinsic factors including hormones, growth factors, pharmacological agents, and mechanical stimuli (1). The regulation of NHE1 by these external stimuli is thought to be exerted through the action of a variety of signaling molecules including calcineurin B homologous protein (2, 3), calmodulin (4, 5), low molecular mass GTPases of the Ras and Rho family (6–8), p42/44 mitogen-activated protein kinases (9), p90 ribosomal S6 kinase (10), 14-3-3 protein (11), Nck-interacting kinase (12), and phosphatidylinositol 4,5-bisphosphate (13). However, the detailed mechanism through which these events occur remains unknown.

Among these factors, CHP1 can serve as an essential cofactor and is required by at least three NHE isoforms (NHE1–3) to express high physiological levels of exchange activity (3). It was shown that CHP1 bound directly to the juxtamembrane region of the C-terminal cytoplasmic domain. When GFP-CHP1 and NHE1–3 were co-expressed, it was found that GFP-CHP1 was mostly localized at the cell surface, whereas co-expression of CHP1 and a CHP1 binding-defective NHE1 mutant failed to show co-localization, implying that NHE1 is a principal target of CHP1 (3). In addition to reduced activity in the neutral pH range, the CHP1 binding-defective NHE1 mutant showed a marked reduction in pH_i sensitivity (~0.7 pH unit acidic shift) that subsequently abolished various NHE1 regulatory responses. Furthermore CHP1 deprivation resulted in marked reduction (>90%) of NHE1 activity (3). These observations suggest that the association of NHE1 with CHP1 is critical for activity and the maintenance of NHE1 pH_i sensitivity (14).

CHP1 consists of four EF-hands, the primary sequence of which is homologous to calmodulin (CaM) and calcineurin B

² The abbreviations used are: pH_i, intracellular pH; HSQC, heteronuclear single quantum coherence; NOE, nuclear Overhauser effect; NOESY, NOE spectroscopy; TOCSY, total correlation spectroscopy; CANDID, combined automated NOE assignment and structure determination module; CaM, calmodulin; CNB, calcineurin B; NHE, Na⁺/H⁺ exchanger; CHP, calcineurin B homologous protein; CNA, calcineurin A; Ni-NTA, nickel-nitrilotriacetic acid; GST, glutathione S-transferase; CHAPS, 3-[(3-cholamidopropyl)dimethylammonio]-1-propanesulfonic acid; r.m.s., root mean square; Kv, voltage-gated potassium channel; KChIP, Kv-interacting protein; PIP₂, phosphatidylinositol 4,5-bisphosphate.

Supplemental Material can be found at:
<http://www.jbc.org/cgi/content/full/M604092200/DC1>

Solution Structure of the NHE1-CHP1 Complex

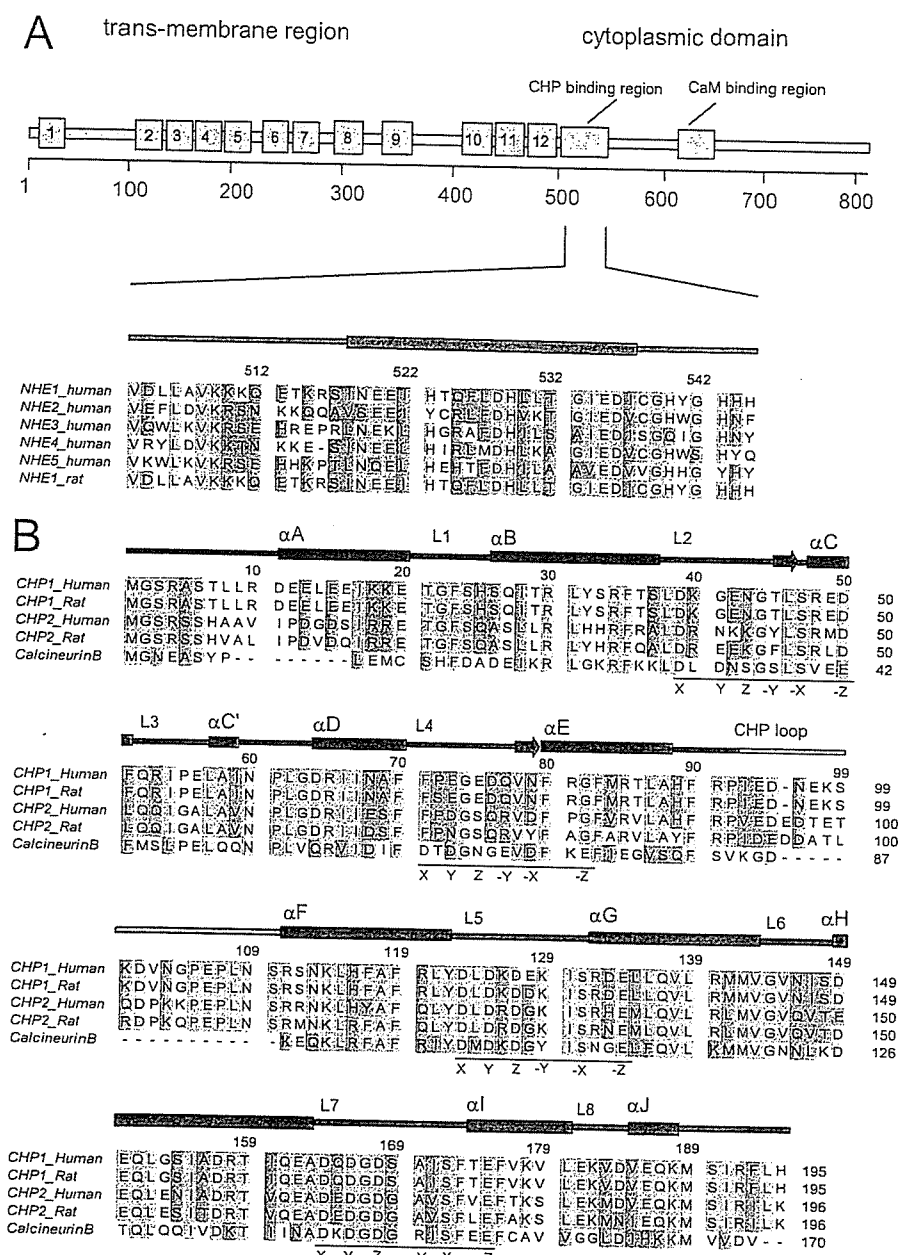


FIGURE 1. Multiple sequence alignments of NHE1 and CHP1. A, domain structure and alignment of NHE1. B, alignment of CHP1, CHP2, and human calcineurin B. In A and B, sequence alignment was performed using ClustalW. Secondary structure elements of the proteins are shown schematically at the top of the alignments. N- and C-terminal domains of CHP1 are colored in blue and magenta, respectively, for clarity. Conserved and semiconserved residues are colored in yellow and green, respectively. The 12-residue motif involved in the EF-hand is underlined, and key residues are indicated as X, Y, Z, -Y, -X, and -Z.

(CNB), possessing 31 and 41% sequence identity, respectively (Fig. 1B). It is well known that all CaM and CNB EF-hands can bind Ca^{2+} . However, CHP1 EF-1 and EF-2 are ancestral and do not bind Ca^{2+} under physiological conditions, whereas EF-3 and EF-4 bind two Ca^{2+} ions with high affinity (~ 90 nM) based on the $^{45}Ca^{2+}$ binding experiments for several CHP1 mutants (14). Complex formation between CHP1 and the CHP1 binding domain of NHE1 resulted in a marked increase in Ca^{2+} binding affinity ($K_d = \sim 2$ nM) (14). This suggests that CHP1 constitutively contains two Ca^{2+} ions when associated with NHE1 in cells (14).

(CNA), CNB, and other related four-EF-hand proteins are also discussed.

EXPERIMENTAL PROCEDURES

Sample Preparation—The NHE1-CHP1 complex was co-expressed and co-purified. DNA encoding NHE1 was cloned into the pET24a vector (Novagen), and CHP1 was subcloned into pET11a (Novagen), which produces recombinant protein with a hexahistidine (His_6) sequence at the C terminus. The proteins were co-overexpressed in *Escherichia coli* BL21(DE3) cells. Uniformly ^{15}N - and $^{15}N/^{13}C$ -labeled proteins were prepared by

Interestingly CHP1 has been reported to exhibit multiple functions. It was initially identified as a protein (p22) involved in vesicular transport (15) and the inhibition of calcineurin phosphatase activity (16). It was also found to interact with microtubules (17), DRAK2 (death-associated protein kinase-related apoptosis-inducing protein kinase 2) (18) and KIF1B β 2 (kinesin family 1B β 2) (19).

A second CHP isoform, CHP2, with 61% sequence identity was also identified and found to be involved in the maintenance of abnormally high pH_i in malignantly transformed cells. CHP2 is expressed at a relatively high level in malignantly transformed cells and in rat small intestine, suggesting that it plays a specific role in this tissue (20). In addition, tescalcin, an EF-hand protein closely related to CNB, that interacts with the cytoplasmic region of NHE1 has been identified (21, 22).

The crystal structure of NHE1-unbound rat CHP1 was recently determined and revealed that the overall structure is similar to CNB where Ca^{2+} ions are coordinated within EF-3 and EF-4. However, the interaction mechanism between NHE1 and CHP1 remains unknown (23).

Here we report on the solution structure of the cytoplasmic region of NHE1 bound to CHP1 as determined by NMR. Details of the NHE1-CHP1 interaction are described. We present mutational binding data to delineate the significance of the interactions observed in the complex. Based on the structure, we suggest a role for CHP1 in terms of NHE1 activation. Comparisons of the binding mode between NHE1-CHP1 and calcineurin A

growing bacteria in minimal medium containing $^{15}\text{N}_4\text{Cl}$ with or without [$^{13}\text{C}_6$]glucose. Uniformly $^{15}\text{N}/^{13}\text{C}$ -labeled and fractionally deuterated protein sample was prepared using medium containing 60% $^2\text{H}_2\text{O}$. The NHE1-CHP1 complex was purified using a standard Ni-NTA affinity column protocol (Qiagen). Further purification was performed by gel filtration using Superdex 200 (GE Healthcare). NMR samples contained 0.5–0.9 mM protein in 50 mM Tris- d_7 buffer (pH 6.9), 1 mM dithiothreitol- d_{10} , 30 mM KCl in $\text{H}_2\text{O}/^2\text{H}_2\text{O}$ (9:1) or $^2\text{H}_2\text{O}$.

NMR Spectroscopy—NMR data were recorded at 37 °C on Bruker AVANCE 500 and DRX 800 NMR spectrometers. Resonance assignments for ^1H N, ^{15}N , $^{13}\text{C}\alpha$, $^{13}\text{C}\beta$, and $^{13}\text{C}'$ nuclei for the CHP1-NHE1 complex were obtained through the following ^2H -decoupled, triple resonance spectra applied to a fractionally deuterated $^{15}\text{N}/^{13}\text{C}$ -labeled sample: three-dimensional HNCACB/HN(CO)CACB (24) and three-dimensional HN(CA)CO/HNCO experiments (25, 26). Side-chain ^1H and ^{13}C resonances were assigned on a fully protonated sample or a fractionally deuterated $^{15}\text{N}/^{13}\text{C}$ -labeled sample using three-dimensional C(CO)NH, three-dimensional H(CCO)NH, four-dimensional HC(CO)NH, and three-dimensional HCCH TOCSY (27–29). Stereospecific assignment of leucine and valine methyl groups were obtained from a Constant Time- $^1\text{H}/^{13}\text{C}$ HSQC spectrum of a 15% ^{13}C -labeled sample (30). $^1\text{H}\alpha$ and $^1\text{H}\beta$ resonance assignments were supplemented with three-dimensional H(CACO)NH (31), ^{15}N -edited TOCSY-HSQC (32), and three-dimensional HBHA(CBCACO)NH (33). Aromatic resonances of both NHE1 and CHP1 were mainly assigned using three-dimensional ^{13}C -aromatic-edited/ ^{15}N -separated NOESY-HSQC, three-dimensional ^{13}C -edited NOESY, ^1H - ^1H TOCSY, and NOESY experiments (32). The assignment was verified using the Constant Time- $^1\text{H}/^{13}\text{C}$ HSQC spectrum of a 15% ^{13}C -labeled sample (30). The following NOESY spectra were recorded for the protonated sample and used to generate distance restraints for structure calculations: three-dimensional ^{15}N -edited NOESY (80-ms mixing time), three-dimensional ^{13}C -edited NOESY (80-ms mixing time), and two-dimensional ^1H NOESY (80-ms mixing time). Slowly exchanging amide protons were identified from a series of two-dimensional ^{15}N HSQC spectra recorded after the H_2O buffer was replaced with $^2\text{H}_2\text{O}$ buffer. All NMR spectra were processed using NMRPipe/NMRDraw (34) analyzed using SPARKY (35).

Structure Calculations—Intramolecular and intermolecular distance constraints were identified in the three-dimensional $^{15}\text{N}/^{13}\text{C}$ -separated NOESY spectra using a $^{15}\text{N}/^{13}\text{C}$ -labeled NHE1-CHP1 sample with mixing times of 80 ms. Backbone hydrogen bond restraints within regular secondary structure elements that were consistent with backbone amide hydrogen/deuterium exchange data were included in the structure calculations. The initial structure calculations were performed by iterative automated assignment of the NOE spectra using CANDID (36) in addition to manually assigned NOE-derived distance restraints. The restraints, leading to converged structures, were subsequently utilized for the iterative automated assignment of all spectra including aromatic residues using CANDID. Finally refinement of the structures (including two Ca^{2+} ions) using XPLOR-NIH (version 2.96) was performed (37). The final structure calculations used a total of 4022 NOE-

Solution Structure of the NHE1-CHP1 Complex

derived distance restraints obtained from the manual and the CANDID-assisted assignments from the ^{15}N - or ^{13}C -edited NOE data. A total of 100 simulated annealing structures were calculated, and 20 structures were selected that possessed no NOE violations greater than 0.5 Å and no dihedral violations greater than 5°. Final structures were evaluated using the program ProcheckNMR (38). Structures and figures were drawn using MOLMOL (39), GRASP (40), and Chimera (41).

Mutagenesis and GST Pulldown Assay—For the binding analyses, CHP1 was expressed as a fusion protein with GST in *E. coli*, which was then subcloned into modified pGEX6P-3 (Novagen) (42). Site-directed mutant proteins were prepared using the QuikChange kit (Stratagene). DNA sequencing confirmed the mutations. Vectors were transformed into BL21(DE3)star (Invitrogen). Cells were grown at 37 °C and then induced with 1 mM isopropyl 1-thio- β -D-galactopyranoside for 12 h at 20 °C. Harvested cells were disrupted via sonication in HEPES (pH 8.0) containing 10% glycerol, 10% sucrose, 1 mM dithiothreitol, and 30 mM KCl. The GST-CHP1 fusion protein was purified using glutathione-Sepharose (GE Healthcare) and a standard protocol except that the equilibrium buffer was changed to 50 mM HEPES buffer (pH 8.0) containing 10% glycerol, 1 mM dithiothreitol, and 30 mM KCl, and the column was washed extensively with 20 mM CHAPS. The effect of mutation on the binding of CHP1 to NHE1 peptides was characterized using a GST pulldown assay. Synthetic NHE1 peptide (residues 514–545 including a hexahistidine sequence at the C terminus) was purchased from Greiner Japan (Tokyo, Japan). Briefly wild-type and CHP1 mutant GST fusion proteins, in addition to GST alone, were incubated for 30 min at 20 °C with NHE1 peptide in binding buffer containing 50 mM HEPES (pH 7.5), 20 mM CHAPS, 10% glycerol, 1 mM Pefabloc, and 1 mM dithiothreitol. GST protein-bound Sepharose beads were washed extensively with binding buffer. Proteins were resolved by 12% NuPAGE (Invitrogen) and blotted onto membranes, and then His-NHE1 was analyzed with Ni-NTA-conjugated alkaline phosphatase (Promega) and Western Blue substrate (Promega). Quantification was represented as the average value of experiments performed in triplicate.

RESULTS AND DISCUSSION

Structure Determination—To better understand the mechanism pertaining to CHP1-regulated NHE1 activity, the solution structure of unmyristoylated CHP1 complexed with the cytoplasmic region (503–545) of NHE1 was determined by NMR spectroscopy. Our structural studies were initially hampered by the fact that NHE1-free CHP1 tended to aggregate during NMR measurements, and the CHP1-unbound cytoplasmic region (503–545) of NHE1 readily degraded during the expression and purification steps. Consequently NMR structural analysis of co-expressed and co-purified samples was undertaken. Co-expression of CHP1 and NHE1-(503–545) produced a stable complex for structural studies and showed no significant degradation and aggregation for several weeks.

The ^1H - ^{15}N HSQC spectrum of NHE1-unbound CHP1 displays many broadened peaks presumably due to formation of a dimer, multimer, or an equilibrium between these states in solution. In contrast, the HSQC spectrum of ^{15}N -labeled CHP1

Solution Structure of the NHE1-CHP1 Complex

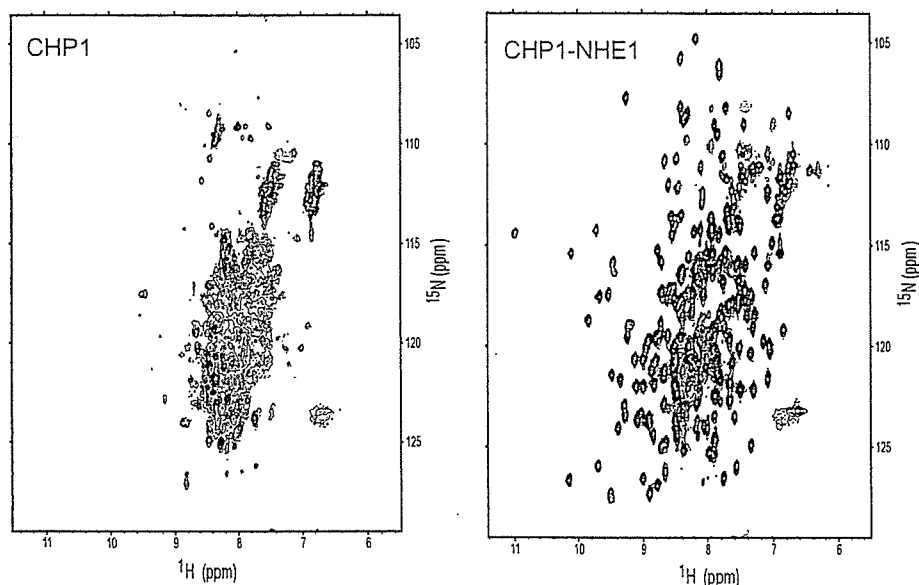


FIGURE 2. ^1H - ^{15}N HSQC spectra of ^{15}N -labeled NHE1-free CHP1 (left image) and ^{15}N -labeled NHE1-(503-545)-CHP1 complex (right image). These spectra were obtained with 0.3 mm samples at pH 6.9 and 37 °C recorded on the AVANCE 500.

TABLE 1

Structural statistics for NHE1-CHP1

These statistics represent an ensemble comprising 20 of the lowest energy structures obtained from 150 starting structures. Structure calculations were performed using XPLOR-NIH version 2.9.6.

Total number of distance constraints	4242
Long range ($ i - j > 4$)	589 (inter: 134)
Middle range ($ i - j = 2, 3, 4$)	874
Short range ($ i - j = 1$)	1038
Intraresidue	1521
Hydrogen bond constraints (including Ca^{2+} coordination restraints)	110×2
Dihedral constraints	
ψ, ϕ	105, 105
χ^1	17
r.m.s. deviation from experimental constraints ^a	
Distance (Å)	$0.0288 \pm 7 \times 10^{-4}$
Angle (°)	$0.44 \pm 3 \times 10^{-2}$
r.m.s. deviation from idealized covalent geometry	
Bonds (Å)	$0.00248 \pm 6 \times 10^{-5}$
Angles (°)	$0.360 \pm 6 \times 10^{-3}$
Impropers (°)	$0.31 \pm 1 \times 10^{-2}$
XPLOR energy terms (kcal/mol) ^b	
E_{bond}	23 ± 1
E_{angle}	138 ± 5
E_{imp}	28 ± 2
$E_{\text{vdw}(1,1)}$	$-6.6 \times 10^2 \pm 0.2 \times 10^2$
PROCHECK Ramachandran plot (185-254)	
Residues in most favored regions (%)	78.6
Residues in additional allowed regions (%)	18.1
Residues in generously allowed regions (%)	2.9
Residues in disallowed regions (%)	0.4
r.m.s. deviation of mean structure derived from 30 calculated structures	
Backbone (10-92, 108-192, 516-538) (Å)	0.53
All heavy (10-92, 108-192, 516-538) (Å)	1.15

^a None of these structures exhibited distance violations >0.5 or dihedral angle violations $>5^\circ$.

^b $E_{\text{vdw}(1,1)}$ represents the Lennard-Jones energy of the XPLOR energy terms.

complexed with NHE1 is well dispersed with favorable line shapes (Fig. 2), suggesting that the complex essentially adopts an ordered monomeric structure in solution.

Our target complex was ~ 27 kDa in size, assuming a 1:1 complex of CHP1 (22 kDa) and NHE1 (5 kDa). This represented

a relatively large molecular weight in terms of conventional NMR studies. Consequently utilization of triple labeling (^2H , ^{13}C , and ^{15}N) and the recently developed computational methodology, CANDID, was extremely helpful in the structure determination. Sequential backbone assignments and most side-chain assignments were obtained from a 60% $^2\text{H}/^{15}\text{N}/^{13}\text{C}$ -labeled sample using standard triple resonance experiments. Missing ^1H resonances were supplemented using heteronuclear three-dimensional NOESY experiments with $^{15}\text{N}/^{13}\text{C}$ -labeled samples. Resonance assignments of methyl groups were carefully confirmed in a stereospecific manner using two-dimensional Constant Time HSQC spectra recorded for a 15% randomly enriched ^{13}C sample.

Methyl groups for 18 of 24 leucines and nine of 11 valines were stereospecifically assigned. Aromatic ring proton assignments, essential for delineating hydrophobic core and protein-protein interactions, were obtained using two-dimensional TOCSY, two-dimensional NOESY, two-dimensional HCCH(rom) TOCSY, and three-dimensional ^{13}C (rom)-edited ^{15}N -separated NOESY experiments.

NMR spectra including the three-dimensional ^{13}C -edited NOESY spectrum used to monitor inter/intramolecular ^1H - ^1H NOEs were of adequate quality to pursue a structural determination of the NHE1-CHP1 complex. Use of partial deuteration and the almost complete resonance assignment of methyl groups forming the hydrophobic core facilitated an initial determination of the overall protein fold. A high resolution structure was subsequently obtained using CANDID for automated assignments, which included the use of ambiguous NOEs from ^{15}N - and ^{13}C -edited NOESY experiments recorded for ^{15}N - or $^{15}\text{N}/^{13}\text{C}$ -labeled protein samples. An iterative approach was used for assigning NOEs in addition to the manually assigned unambiguous NOEs. The solution structure of the CHP1-NHE1 complex was determined from a total of over 4000 NMR-derived restraints, including 134 intermolecular distance restraints (Table 1). The ensemble of 20 structures in excellent agreement with a large body of experimental data were well defined (Fig. 3A). The r.m.s. deviations of backbone and heavy atoms over residues 518-537 of NHE1 and residues 10-92 and 108-193 of CHP1 were 0.53 and 1.15 Å, respectively. Of the NMR structures determined, the one with the smallest total energy was selected as representative for further discussion. The complex is predominantly α -helical, and the CHP1 helices constitute a cleft. A helix of the cytoplasmic region of NHE1 associates with CHP1 in 1:1 stoichiometry via the cleft (Fig. 3, A and B).

Structure of NHE1—NHE1 forms a five-turn amphipathic helix composed of residues 518-537. Orientation of the NHE1 helix is well defined relative to CHP1, consistent with the large

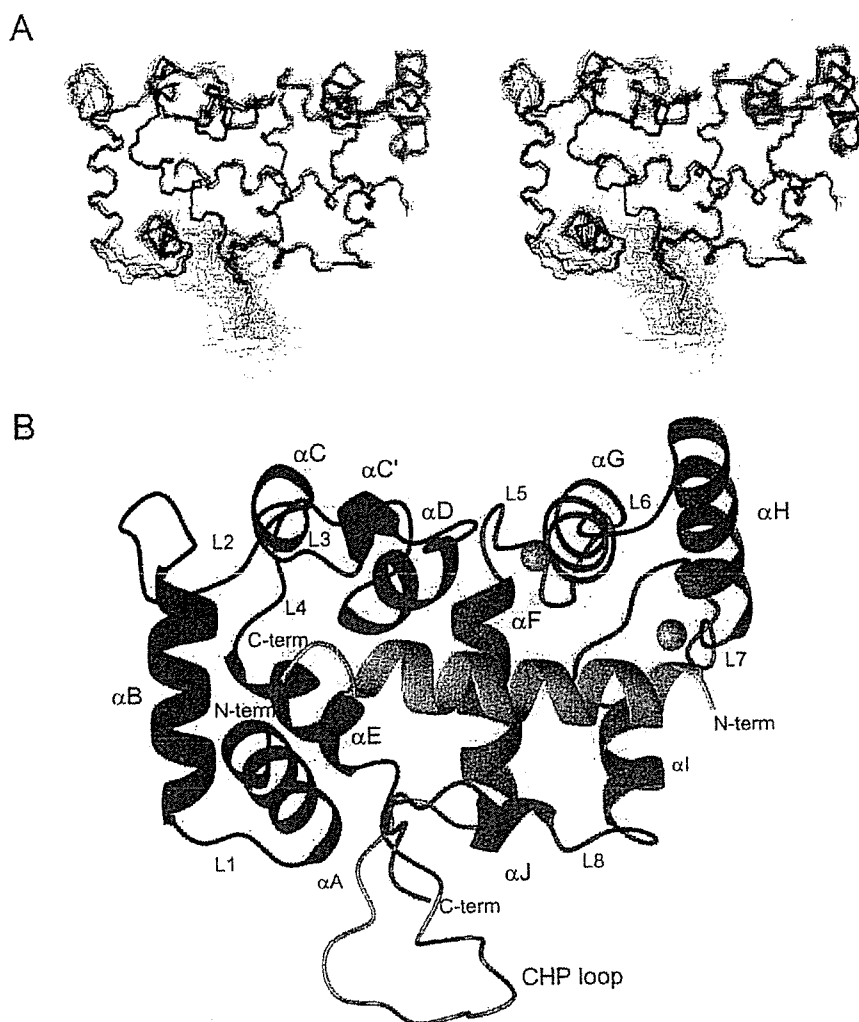


FIGURE 3. Solution structure of the NHE1-CHP1 complex. *A*, stereoview of the backbone superpositions of the final 20 simulated annealing structures of the NHE1-CHP1 complex. *B*, ribbon drawing of the representative NHE1-CHP1 structure complex. *A* and *B*, residues 517–538 of NHE1 and 10–192 of CHP1 are shown. The N- and C-terminal domains of CHP1 are colored in blue and magenta, respectively, and the CHP loop is colored in gray. NHE1 is shown in green. Ca^{2+} ions are shown by gold spheres.

number of intermolecular NOEs detected between CHP1 and NHE1 (Table 1 and Fig. 3A). The N-terminal half of the helix (residues 518–530) binds to the C-terminal domain of CHP1, and the C-terminal half of the helix (residues 531–537) binds to the N-terminal domain of CHP1 (Fig. 4A). Side-chain conformations of the helix are also well defined particularly for apolar residues that make extensive contacts with CHP1. For example, NMR spin-echo difference $^3J_{\text{NC}\gamma}$ and $^3J_{\text{CC}\gamma}$ experiments, which bring about χ_1 rotamer information of aromatic side chain, showed that the His-523 and Phe-526 adopted *g+* and *t* conformations, respectively. The helix exhibits amphipathic character in which the bulky hydrophobic residues Ile-518, Ile-522, His-523, Phe-526, Leu-527, Leu-530, Leu-531, Ile-534, and Ile-537 are clearly confined to one side, and hydrophilic residues are exposed at the other side (Fig. 4B). The hydrophobic residues form a continuous apolar surface (Fig. 4B). The main-chain and side-chain conformations of residues preceding and following the helix, residues 503–517 and 538–545, respectively, are poorly defined in the NMR structure because of the absence

of medium and long range NOEs involving these regions. The narrow resonance linewidths, chemical shift index, and steady state $\{^1\text{H}\}$ - ^{15}N heteronuclear NOE suggest that these regions are unstructured in the complex.

Structure of CHP1—CHP1 is composed of 10 α -helices and a long loop folded into two globular regions representing the N- and C-terminal domains (Fig. 3B). The secondary structure consists of αA (residues 11–22), αB (residues 26–37), αC (residues 48–51), αD (residues 64–70), αE (residues 80–88), αF (residues 111–122), αG (residues 132–143), αH (residues 149–162), αI (residues 174–180), and αJ (residues 185–188) (Figs. 1B and 3B). The N-terminal domain consists of ancestral EF-hands, EF-1 and EF-2, that do not bind calcium under physiological conditions. The EF-1 hand includes helix αB , loop L2, and helix αC followed by loop L3 to the second EF-hand that includes helix αD , loop L4, and helix αE (Figs. 1B and 3B). A long loop region consisting of residues 93–110 connects the N- and C-terminal domains. Because this characteristic long insertion is not found in calcineurin B (Figs. 1B and 3, A and B), we refer to this long loop as the CHP loop. The absence of medium and long range NOEs, a chemical shift index, and $\{^1\text{H}\}$ - ^{15}N heteronuclear NOE value indicate that this region

is flexible in solution. The first EF-hand in the C-terminal domain includes helix αF , loop L5, and helix αG followed by loop L6 and the second EF-hand that consists of helix αH , loop L7, and helix αI (Figs. 1B and 3B).

The four CHP1 EF-hands form a deep hydrophobic pocket, which constitutes the interaction surface for the NHE1 amphipathic α -helix. CHP1 binds to the apolar side of NHE1 with the four EF-hands through a side-by-side manner (Fig. 4A). This contrasts with the well known canonical CaM-target binding mode that represents a wrap-around manner in which two pairs of EF-hands bind to the target IQ motif helix on opposite sides to each other (43, 44).

Although there is modest sequence similarity between CHP1 and CaM, it should be noted that the latter interacts with a large number of proteins with various interaction modes including canonical 1:1 binding and non-canonical 1:1, 1:2, and 2:2 binding (43, 44). It has been suggested that the observed binding versatility of CaM could be derived from the variable positioning of the two domains, linked by a flexible linker, that can

Solution Structure of the NHE1-CHP1 Complex

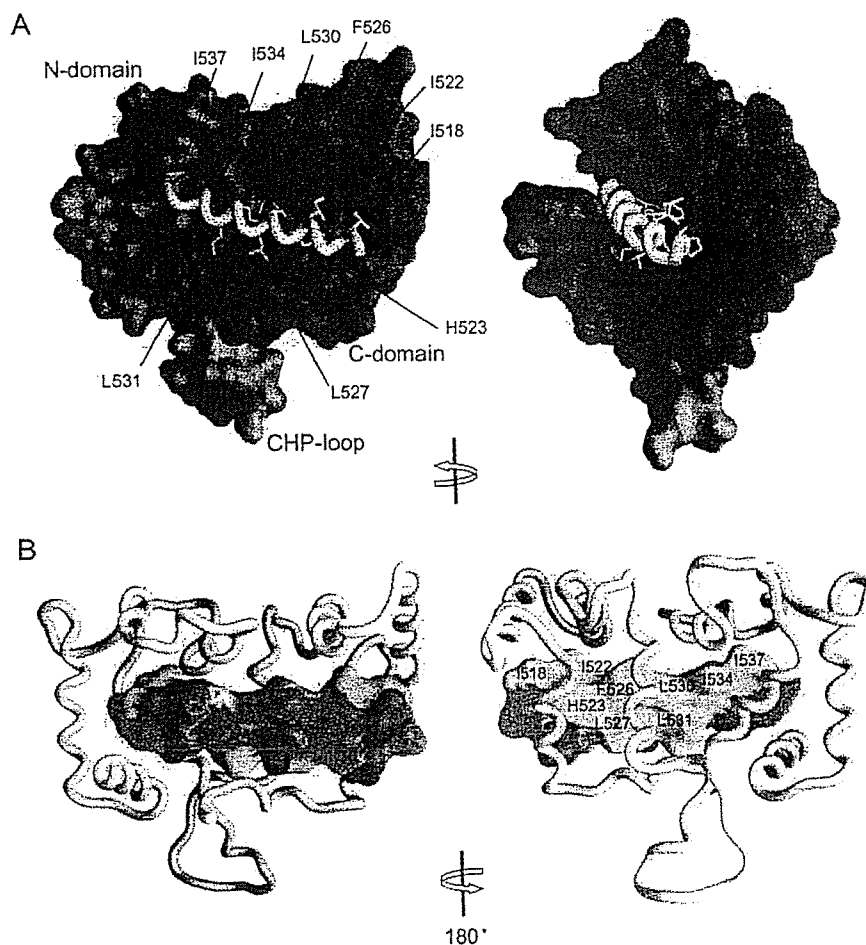


FIGURE 4. Molecular surface of the NHE1-CHP1 complex. *A*, molecular surface of CHP1 and backbone tube representation of NHE1 with yellow stick that shows the hydrophobic side chains. The N- and C-terminal domains of CHP1 are colored in blue and magenta, respectively. *B*, molecular surface of NHE1 and backbone tube representation of CHP1. Hydrophobic, acidic, and polar residues are colored in yellow, red, and blue, respectively.

accommodate different targets. Although target multiplicity has been reported in the case of CHP1, it seems to possess more limited binding modes than CaM. One notable feature of CHP1 that illustrates its difference to CaM has to do with the interdomain interaction. This interaction restricts domain orientation, a phenomenon absent in CaM. In our CHP1 structure, residue Leu-62 of the N-terminal domain participates in a hydrophobic interaction with residues Val-138 and Met-141 of the C-terminal domain, and residue Ala-69 of the N-terminal domain interacts with residue Leu-122 of the C-terminal domain. A side-by-side interaction mediated by four EF-hands has also been reported to take place with voltage-gated potassium channel (Kv)-interacting protein (KChIP) (45) and with CNA-CNB (46, 47) (Fig. 5A).

The atomic r.m.s. difference of well fitted parts between CHP1 complexed with NHE1 and CNB complexed with CNA (Protein Data Bank code 1AUI) is 2.7 Å, indicating that the fit is not very good, although the topology is identical with a high Z-score of 11.8 from a distance matrix alignment (DALI) search. The r.m.s. deviation value improves to 1.7 Å when only the N-terminal domains are superimposed, and it is 1.8 Å when only the C-terminal domains are superimposed. This indicates

that the higher r.m.s. deviation for both domains originates from an interdomain swiveling between NHE1-CHP1 and CNA-CNB, although both proteins bind cognate targets in a side-by-side manner. Similarly domain swiveling was observed between NHE1-bound and NHE1-free CHP1. Swiveling of the N- and C-terminal domains could create a binding surface for cognate targets.

Comparison with Other EF-hands—It is interesting to note that both EF-1 and EF-2 adopt an open conformation in NHE1-bound CHP1 without Ca²⁺. This is especially evident when comparing the angles between the EF-hand helices. In Fig. 5B, a graphical view of the interhelical angles between the first and second helices of EF-1 and EF-2 of apoCaM (a typical closed conformation), Ca²⁺-CaM (a typical open conformation, CNB), KChIP1, NHE1-bound CHP1, and NHE1-free CHP1 is displayed using a vector geometry mapping method (48, 49). The first helices of the EF-hands are superimposed along the z axis, and the spatial localization of the second helices are shown as a cylinder. This indicates that both EF-1 and EF-2 of NHE1-bound CHP1 adopt an open conformation, whereas EF-1 and EF-2 of NHE1-

free CHP1 adopt an open and semiopen conformation, respectively (Fig. 5B and supporting information S1). This implies that EF-1 and EF-2 adopt a constitutively open conformation. However, it should be noted that the hydrophobic cleft of the N-terminal domain of free CHP1, as revealed by the crystal structure, is plugged by additional linker residues (Leu-Ala-Ala-Ala-Leu-Glu-His) (23) derived from the expression vector, partly mimicking the NHE1 helix (Fig. 5A). Binding of the vector-derived linker might have facilitated adoption of the open and semiopen conformations of EF-1 and EF-2, respectively. Therefore, the possibility of a "closed to open" conformational transition of EF-1 and EF-2 remains to be evaluated.

The binding of EF-hands in an open conformation without Ca²⁺ to target molecules has been found following crystal structure investigations of a Kv-KChIP1 in which the Kv fragment is covalently linked to the C terminus of KChIP1 (45). In this case, the Kv fragment binds to EF-1 and EF-2 of the N-terminal domain of KChIP1 through hydrophobic interactions (Fig. 5A). Of particular note, KChIP1 forms a dimer utilizing the surface formed by the Kv peptides and helix 10 of the C-terminal domain of KChIP1 in contrast to NHE1-CHP1, which exists as a monomer (Fig. 5C). The interhelix angles of EF-1 and EF-2

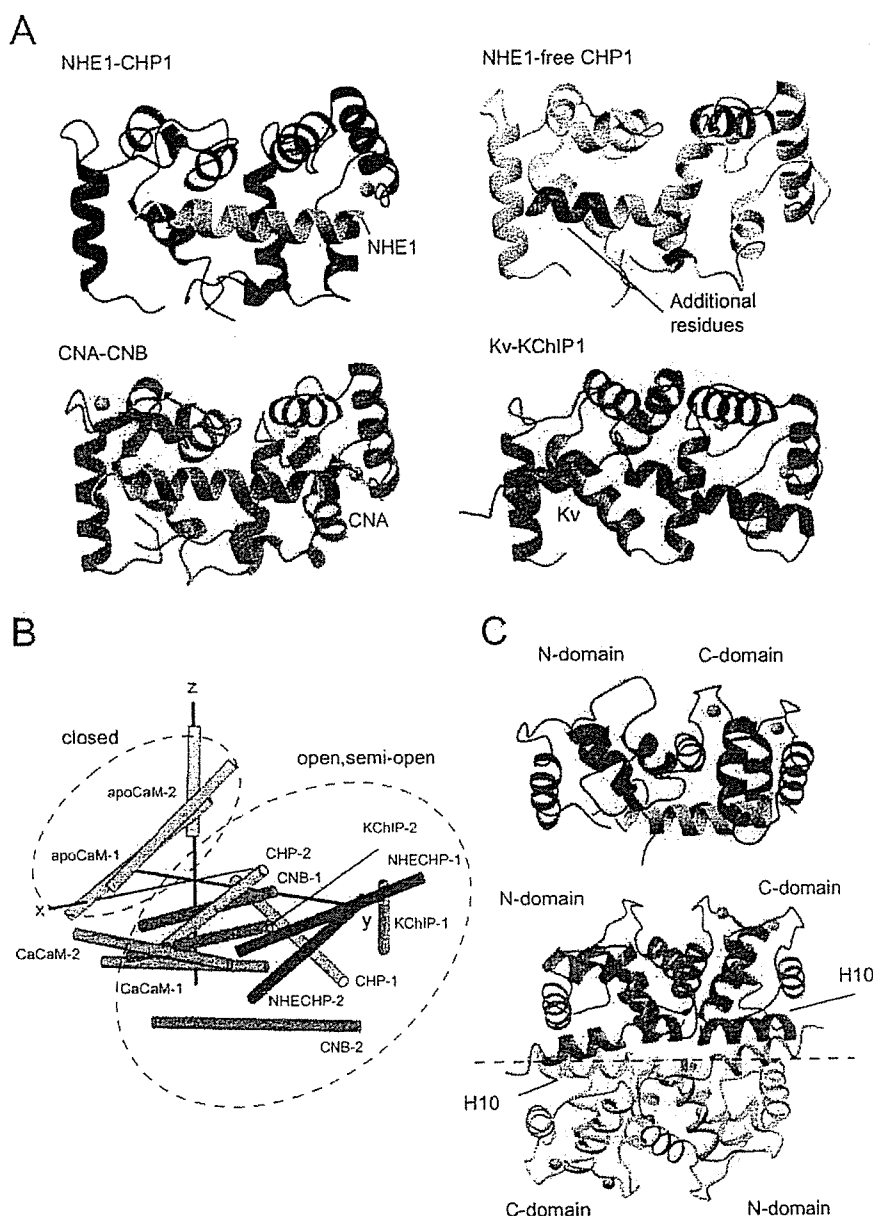


FIGURE 5. Structure comparisons. *A*, ribbon representation of NHE1-CHP1, rat NHE1-free CHP1 (2CT9) in which additional residues from the expression vector interacting with the N-terminal domain (LAAALEH) are depicted in *magenta*, CNA-CNB (1AU1), and Kv-KChIP1 (1S6C). Protein Data Bank entries are shown in parentheses. *B*, vector geometry mapping of EF-1 and EF-2 apocalmodulin, Ca²⁺-calmodulin, calcineurin B, Kv-KChIP1, NHE1-bound CHP1, and NHE1-free CHP1 are denoted as "apoCaM," "CaCaM," "CNB," "KChIP," "NHECHP," and "CHP," respectively. *Hyphenated numbers 1 and 2* denote EF-1 and EF-2, respectively, for each protein. *C*, comparison of the KChIP1 dimer and CHP1 structures colored in *brown* and *blue*, respectively. Bound Kv and NHE1 are colored in *pink* and *green*, respectively. The dimer interface of KChIP1 is shown as a *dashed line*, and one molecule of the dimer is shown in *light colors*. KChIP1 and CHP1 are depicted in the same orientation. In *A* and *C*, the N- and C-terminal regions, αA , and the CHP loop of CHP1 are not shown in the comparison for reasons of clarity.

are 82° and 72°, respectively (supporting information S1), which are slightly larger than those of CHP1. A dimeric interaction in addition to binding of the Kv fragment may contribute to broadening of the cleft constituted by EF-1 and EF-2.

CHP1 shares 18% sequence identity with KChIP1, and the folding topology is almost identical (Fig. 5A). However, the target recognition mechanism differs from that of KChIP1 as judged from the determined structures. KChIP1 belongs to the

extensively studied NCS1 family, which act as important regulators of various functions among certain higher eukaryotes (50). We propose that the NHE1-CHP1 interaction represents a novel binding mode utilized throughout the four-EF-hand proteins, which constitute a distinct subfamily to the NCS1 family. Furthermore detailed comparison of the binding mode of CHP1 and CNB will be presented below.

The CHP1-NHE1 Interface—The protein-protein interface consists of an extensive hydrophobic concave CHP1 undersurface and an apolar NHE1 surface. The concave undersurface spans both the N- and C-terminal domains of CHP1. The total surface area buried at the interface is 2338 Å², slightly smaller than the value of 2625 Å² for the interface between CNA and CNB (Protein Data Bank code 1AU1). Approximately more than 90% of the total buried surface area between NHE1 and CHP1 is hydrophobic, similar to the complexed structure of CNA and CNB.

The interface formed between NHE1 and CHP1 includes methyl-containing and aromatic hydrophobic residues. The residues of the N-terminal domain of CHP1, Ala-69, Phe-90, Ile-66, Thr-86, Leu-87, Phe-35, and Leu-54, comprise a hydrophobic cleft that interacts with the apolar surface formed by the side chains of NHE1 residues Leu-530, Ile-534, and Ile-537. Additionally the side chain of NHE1 Leu-531 expands the hydrophobic area interacting with CHP1 Phe-90 (Fig. 6A). The C-terminal domain residues of CHP1, Ala-163, Thr-159, Leu-139, Leu-135, Tyr-122, Phe-176, Ile-171, Phe-117, Ala-118, and Leu-121, constitute a continuous hydrophobic cleft that interacts with the N-terminal portion of NHE1 helix residues Ile-518, Ile-522, and Phe-526, which protrude at the apolar side. NHE1 residues Leu-527 and His-523 make additional hydrophobic contact with CHP1 residues Tyr-122, Phe-176, and Val-185 (Fig. 6A). These interface-forming hydrophobic residues are well conserved within NHE and CHP isoforms, reflecting the importance of these interactions (Fig. 1B). Furthermore the acidic side chain of Asp-528 at the center of NHE1 helix seems to form a salt bridge with the basic side

Solution Structure of the NHE1-CHP1 Complex

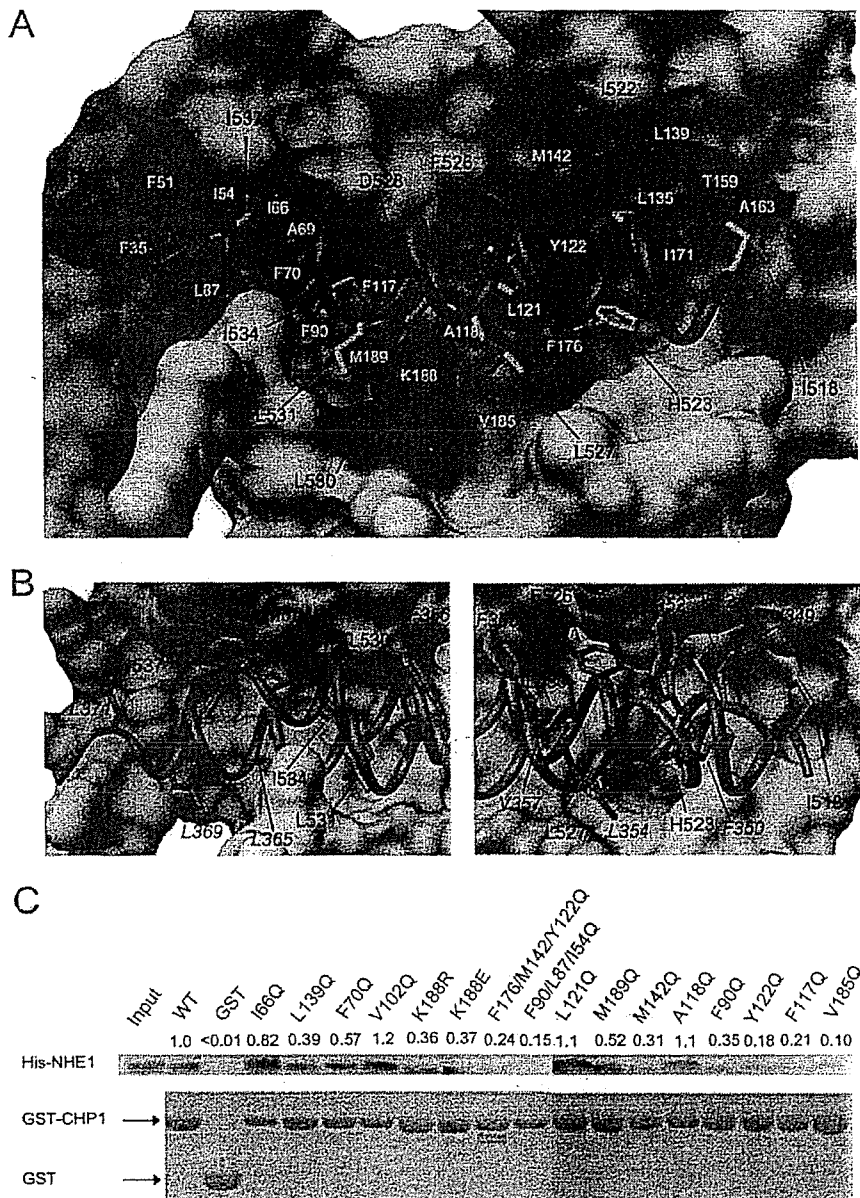


FIGURE 6. Noncovalent interactions at the NHE1-CHP1 interface and contribution to the overall stability of the complex. *A*, molecular surface of CHP1 and backbone tube representation of NHE1 with yellow and red sticks that show hydrophobic and acidic side chains, respectively. Hydrophobic and basic surface residues of CHP1 are colored in orange and blue, respectively. *B*, superposition of NHE1-CHP1 and CAN-CNB (Protein Data Bank code 1AU1). NHE1 and CNA are shown in green and magenta, respectively, and the molecular surface of only CHP1 is depicted for clarity. Complex-forming hydrophobic residues of NHE1 and CNA are shown as sticks and are labeled. CNA residues are represented in italics. The left-hand image and the right-hand image are close-up views of the N- and C-terminal domains. *C*, binding of His-NHE1 peptide to GST-CHP1 mutants in an *in vitro* pull-down assay. Bound peptide was separated via SDS-PAGE, blotted to a membrane, and then visualized using Ni-NTA-conjugated alkaline phosphatase (top). The amount of GST-CHP1 mutant used was estimated by Coomassie Blue staining (bottom) for calibration. The binding of NHE1 peptide to GST-CHP1 mutants was quantified and expressed as a ratio of binding of wild-type protein at the top of the gel images.

chain of CHP1 Lys-188. The presence of this interaction was observed in 10 of the final 20 NMR structures derived using the MONSTER server (51), which identifies interacting residues and assigns the nature of those interactions based on the structure. These residues are also conserved (Figs. 1, *A* and *B*, and 6*A*).

NHE1 binding orientation relative to CHP1 is probably established by surface complementarity that comprises the hydrophobic surfaces of NHE1 and CHP1. NHE1 side chains of

Ile-534 and Ile-537 protrude into the shallow cleft made by the CHP1 N-terminal domain. Meanwhile NHE1 aromatic side chains of His-523 and Phe-526 protrude into the deep cleft of the CHP1 C-terminal domain (Fig. 6*A*). This deep cleft allows enough space so that they can interact with the bulky side chains of NHE1. The difference between the shapes of the domains is critical for NHE1 binding orientation.

Notably the shape of the interaction surfaces of NHE1-CHP1 and CNA-CNB differs. The spatial arrangement of NHE1 and CNA residues that contribute to form the interaction surfaces differs for each (Fig. 6*B*). Only Val-349, Phe-350, and Val-357 of CNA are located at equivalent positions to Ile-522, His-523, and Leu-530 of NHE1 unlike other residues. Clearly Trp-352 and Phe-356 of CNA that interact with the roof of the hydrophobic cleft formed by CNB are missing in NHE1. Furthermore the interactions mediated by the C-terminal stretch region of CNA, where Leu-369 and Leu-371 protrude, are absent in NHE1. On the other hand, the corresponding residues to Phe-526 and Ile-518 of NHE1 are absent in CNA.

Consequently the interaction mechanism dominated by hydrophobic interactions through amphipathic helices and four EF-hands is common in both complexes, but their shape differs. This surface complementarity in terms of a knobs-into-hole mode of interaction defines the binding specificity of these proteins, although the folding topology is identical.

Correlation with Mutagenesis Studies—The solution structure of the CHP1-NHE1 complex is essentially consistent with previous mutagenesis studies concerning

NHE1. Co-immunoprecipitation experiments showed that the 4Q mutant of NHE1, in which Phe-526, Leu-527, Leu-530, and Leu-531 are substituted with glutamine, displayed no binding to CHP1, whereas the I518Q/I522Q NHE1 double mutant displayed some binding albeit with decreased affinity (3). Our structure determination revealed that Phe-526, Leu-527, Leu-530, and Leu-531 form a hydrophobic core that interacts with the center of the hydrophobic cleft of the C-terminal domain of

Solution Structure of the NHE1-CHP1 Complex

CHP1, whereas Ile-518 and Ile-522 interact with the rim of the hydrophobic cleft of the C-terminal domain of CHP1 (Figs. 4B and 6A). Deletion mutagenesis indicated that NHE1 (residues 510–575) retained binding affinity similar to the wild-type protein, implying that the juxtamembrane region of NHE1 comprising residues 503–509 is unimportant for CHP1 binding (3). These residues were found to be unstructured in the present study and form no direct contact with NHE1.

The binding activity of NHE1 (residues 530–656) lacking the N-terminal segment was found to be completely impaired (3). Our NHE1-CHP1 complex structure shows that an absence of residues preceding Leu-530 results in almost complete loss of interaction between NHE1 and the C-terminal domain of CHP1, whereas the many hydrophobic interactions mediated by NHE1 residues Leu-530, Leu-531, Ile-534, and Ile-537 are retained (Fig. 6A). This indicates that interaction of the N-terminal residues of NHE1 and the C-terminal domain of CHP1 is indispensable in maintaining the NHE1-CHP1 complex. Namely this part of the interaction plays a dominant role in NHE1-CHP1 complex formation.

CHP1 was subjected to site-directed mutagenesis in an effort to reveal detailed individual contributions of interfacial residues toward the overall stability of the NHE1-CHP1 complex. We selected three categories of residues in CHP1: 1) residues that comprise the floor of the hydrophobic pocket, Phe-70, Phe-90, Phe-117, Ala-118, Leu-121, Tyr-122, and Met-189; 2) residues forming the rim of the pocket, Ile-66, Leu-139, Met-142, and Val-185; and 3) a residue forming the salt bridge, Lys-188. A noninteracting solvent-exposed residue, Val-102, as the positive control and a triple mutation involving hydrophobic residues Phe-90/Leu-87/Leu-54 and Phe-176/Met-142/Tyr-122 as the negative control were prepared.

Dramatic effects were observed in terms of CHP1 binding to NHE1 with mutations F117Q, Y122Q, and V185Q (Fig. 6C). We expected the floor-forming residues located at the bottom of the cleft to be critical for the interaction, but the rim-forming residue Val-185 showed significant reduction similar to the negative control. Based on the solution structure of the NHE1-CHP1 complex, it was appeared that Phe-117, Tyr-122, and Val-185 were confined to the C-terminal domain of CHP1 and were packed against the apolar side of NHE1. This suggests that the C-terminal hydrophobic cleft represents a mutation hot spot, implying that it plays a key role in the NHE1-CHP1 interaction. This result is consistent with the NHE1 deletion result indicating that interaction between the N-terminal segment of NHE1 and the C-terminal domain of CHP1 is dominant. This represents a unique feature of the NHE1-CHP1 interaction.

Although mutation of residues possibly involved in salt bridge formation such as K188E and K188R resulted in a marked decrease in binding interaction, the effect was not strong, and the charge-reversing effect of K188E was unclear. Thus, it appears that although this salt bridge contributes to NHE1-CHP1 complex formation, it is not the main force possibly because this bond is exposed to solvent (Fig. 6A), and therefore solvation could weaken the strength of the interaction.

Role of CHP1—NMR investigations of NHE1 complexed with CHP1 revealed that the juxtamembrane region comprising res-

idues 503–517 was unstructured in solution. This region is rich in basic residues with a previous study reporting that NHE1 comprising residues 506–576 bound to PIP₂ *in vitro* (13). In addition, residues 513–520 and 556–564 might represent PIP₂ binding sites (13). Accordingly it is likely that this juxtamembrane region (residues 503–517) following the last transmembrane helix (H12, residues 478–499) is incapable of forming a continuous straight helical structure into the cytoplasm due to interaction with the membrane. Rather the overall structure of NHE1 presumably turns or bends toward the cytoplasmic membrane following a PIP₂-mediated interaction. Assuming that flanking regions of the helix, residues 513–520 and 556–564, attach to the membrane (PIP₂) (13), the helix and CHP1 should be located immediately beneath the cytoplasmic membrane.

Furthermore it has been reported that NHE1 acts as a scaffold protein linked to actin filaments via ezrin-radixin-moesin proteins in addition to possessing function as an ion exchanger (52, 53). Our NMR studies revealed that the cytoplasmic helix-forming residues of NHE1 comprise residues 518–537, which showed little overlap from the previously reported ezrin-radixin-moesin binding region (512–520 and 550–565). This ensures simultaneous binding of NHE1 to CHP1 and ezrin-radixin-moesin proteins.

The juxtamembrane region of NHE1 forms a particular tertiary or quaternary structure that is mediated by interactions with the membrane (PIP₂), CHP1, and ezrin-radixin-moesin proteins. The overall structure of the juxtamembrane region might play an important role in NHE1 activity. The 90% loss in activity following CHP1 depletion might be due to disruption of the structure of the cytoplasmic region of NHE1 around the membrane. In fact, although this represents *in vitro* evidence, the amphipathic helix is disrupted in the absence of CHP1 based on the CD and NMR data (supporting information S2 and S3).

Possible Mode of Regulation—CHP1 deprivation resulted in impaired regulation of NHE1 following external stimuli, implying that CHP1 acts as regulator of NHE1 by involvement in the processing of intracellular signals derived from external stimuli. However, the regulatory mechanism remains unclear. Although it was reported that CHP1 is an *N*-myristoylated protein, CHP1 does not exert myristoyl switching in a Ca²⁺-dependent manner under normal physiological conditions because EF-3 and EF-4 constitutively bind Ca²⁺ ions where *N*-myristoylation was not required for NHE1 binding, activation, or localization (14).

Of particular note, it was reported that CHP1 is a phosphorylated protein, although the phosphorylation sites were not determined. According to the phosphorylation prediction server NetPhos (54), the CHP1 sequence contains potential phosphorylation sites located at residues Thr-36, Ser-37, Ser-47, Ser-131, and Ser-172 (score, >0.8). Similarly the phosphorylation server Scansite (55) identified potential phosphorylation sites located at residues Thr-36, Ser-37, and Ser-172 (score, >0.5). From the determined NHE1-CHP1 structure, residues Thr-36, Ser-37, and Ser-172, predicted by both servers as potential phosphorylation sites, are located at the terminal part of the EF-hand helix or its flanking loop where the side chains of

Solution Structure of the NHE1-CHP1 Complex

the aforementioned residues are exposed to the protein surface reinforcing the possibility of phosphorylation. Phosphorylation-induced conformational changes in CHP1 and the subsequent regulation of NHE1 activity are interesting areas that remain to be investigated.

Conclusion—We have determined the solution structure of the cytoplasmic region of NHE1 complexed with CHP1. Although previous biochemical analyses suggested that the hydrophobic residues of NHE1 were likely to interact with CHP1, the present study has delineated the structural basis for this interaction. The solution structure provides concrete evidence that the cytoplasmic region of NHE1 forms an amphipathic helix that interacts directly with the large concave undersurface of CHP1. This helix is disrupted in the absence of CHP1; thus the loss in activity following CHP1 depletion might be due to disruption of the structure of the juxtamembrane region of NHE1. Our structure provides a first step toward understanding the regulation of NHE1 activity. Moreover it revealed a novel target binding mechanism mediated by four EF-hands. These findings should facilitate future studies aimed at understanding the mechanism underlying recognition utilized by EF-hand proteins that are engaged in signal transduction pathways and many other molecular and cellular events. During the initial review of our manuscript, a study appeared that describes a crystal structure of the NHE1 peptide complexed with CHP2 containing Y^{3+} ions instead of Ca^{2+} (56).

Acknowledgments—We are grateful to Momoko Yoneyama, Hiroko Kinoshita, and Junko Tsukamoto of the Nara Institute of Science and Technology for technical assistance and Kokoro Hayashi for help in sample preparation.

REFERENCES

- Orlowski, J., and Grinstein, S. (2004) *Pfluegers Arch. Eur. J. Physiol.* 447, 549–565
- Lin, X., and Barber, D. L. (1996) *Proc. Natl. Acad. Sci. U. S. A.* 93, 12631–12636
- Pang, T., Su, X., Wakabayashi, S., and Shigekawa, M. (2001) *J. Biol. Chem.* 276, 17367–17372
- Bertrand, B., Wakabayashi, S., Ikeda, T., Pouyssegur, J., and Shigekawa, M. (1994) *J. Biol. Chem.* 269, 13703–13709
- Wakabayashi, S., Bertrand, B., Ikeda, T., Pouyssegur, J., and Shigekawa, M. (1994) *J. Biol. Chem.* 269, 13710–13715
- Dhanasekaran, N., Prasad, M. V., Wadsworth, S. J., Dermott, J. M., and van Rossum, G. (1994) *J. Biol. Chem.* 269, 11802–11806
- Hooley, R., Yu, C. Y., Symons, M., and Barber, D. L. (1996) *J. Biol. Chem.* 271, 6152–6158
- Voyno-Yasenetskaya, T., Conklin, B. R., Gilbert, R. L., Hooley, R., Bourne, H. R., and Barber, D. L. (1994) *J. Biol. Chem.* 269, 4721–4724
- Bianchini, L., L'Allemain, G., and Pouyssegur, J. (1997) *J. Biol. Chem.* 272, 271–279
- Takahashi, E., Abe, J., Gallis, B., Aebersold, R., Spring, D. J., Krebs, E. G., and Berk, B. C. (1999) *J. Biol. Chem.* 274, 20206–20214
- Lehoux, S., Abe, J.-i., Florian, J. A., and Berk, B. C. (2001) *J. Biol. Chem.* 276, 15794–15800
- Yan, W., Nehrke, K., Choi, J., and Barber, D. L. (2001) *J. Biol. Chem.* 276, 31349–31356
- Aharonovitz, O., Zaun, H. C., Balla, T., York, J. D., Orlowski, J., and Grinstein, S. (2000) *J. Cell Biol.* 150, 213–224
- Pang, T., Hisamitsu, T., Mori, H., Shigekawa, M., and Wakabayashi, S. (2004) *Biochemistry* 43, 3628–3636
- Barroso, M. R., Bernd, K. K., DeWitt, N. D., Chang, A., Mills, K., and Sztul, E. S. (1996) *J. Biol. Chem.* 271, 10183–10187
- Lin, X., Sikkink, R. A., Rusnak, F., and Barber, D. L. (1999) *J. Biol. Chem.* 274, 36125–36131
- Timm, S., Titus, B., Bernd, K., and Barroso, M. (1999) *Mol. Biol. Cell* 10, 3473–3488
- Matsumoto, M., Miyake, Y., Nagita, M., Inoue, H., Shitakubo, D., Take-moto, K., Ohtsuka, C., Murakami, H., Nakamura, N., and Kanazawa, H. (2001) *J. Biochem. (Tokyo)* 130, 217–225
- Nakamura, N., Miyake, Y., Matsushita, M., Tanaka, S., Inoue, H., and Kanazawa, H. (2002) *J. Biochem. (Tokyo)* 132, 483–491
- Pang, T., Wakabayashi, S., and Shigekawa, M. (2002) *J. Biol. Chem.* 277, 43771–43777
- Mailander, J., Muller-Esterl, W., and Dedio, J. (2001) *FEBS Lett.* 507, 331–335
- Perera, E. M., Martin, H., Seeherunvong, T., Kos, L., Hughes, I. A., Hawkins, J. R., and Berkovitz, G. D. (2001) *Endocrinology* 142, 455–463
- Naoe, Y., Arita, K., Hashimoto, H., Kanazawa, H., Sato, M., and Shimizu, T. (2005) *J. Biol. Chem.* 280, 32372–32378
- Yamazaki, T., Lee, W., Arrowsmith, C. H., Muhandiram, D. R., and Kay, L. E. (1994) *J. Am. Chem. Soc.* 116, 11655–11666
- Matsuo, H., Kupce, E., Li, H., and Wagner, G. (1996) *J. Magn. Reson. B* 111, 194–198
- Muhandiram, D. R., and Kay, L. E. (1994) *J. Magn. Reson. B* 103, 203–216
- Clowes, R. T., Boucher, W., Hardman, C. H., Domaille, P. J., and Laue, E. D. (1993) *J. Biomol. NMR* 3, 349–354
- Kay, L. E., Xu, G. Y., Singer, A. U., Muhandiram, D. R., and Formankay, J. D. (1993) *J. Magn. Reson. B* 101, 333–337
- Logan, T. M., Olejniczak, E. T., Xu, R. X., and Fesik, S. W. (1993) *J. Biomol. NMR* 3, 225–231
- Neri, D., Szyperks, T., Otting, G., Senn, H., and Wuthrich, K. (1989) *Biochemistry* 28, 7510–7516
- Boucher, W., Laue, E. D., Campbell-Burk, S., and Domaille, P. J. (1992) *J. Am. Chem. Soc.* 114, 2262–2264
- Cavanagh, J., Fairbrother, W. J., Palmer, A. G., III, and Skelton, N. J. (1996) *Protein NMR Spectroscopy*, pp. 301–531, Academic Press, San Diego, CA
- Grzesiek, S., and Bax, A. (1993) *J. Biomol. NMR* 3, 185–204
- Delaglio, F., Grzesiek, S., Vuister, G. W., Zhu, G., Pfeifer, J., and Bax, A. (1995) *J. Biomol. NMR* 6, 277–279
- Goddard, T. D., and Kneller, D. G. (1999) *SPARKY3*, University of California, San Francisco
- Herrmann, T., Guntert, P., and Wuthrich, K. (2002) *J. Mol. Biol.* 319, 209–227
- Schwieters, C. D., Kuszewski, J. J., Tjandra, N., and Clore, G. M. (2003) *J. Magn. Reson.* 160, 65–73
- Laskowski, R. A., Rullmann, J. A., MacArthur, M. W., Kaptein, R., and Thornton, J. M. (1996) *J. Biomol. NMR* 8, 477–486
- Koradi, R., Billete, M., and Wuthrich, K. (1996) *J. Mol. Graph.* 14, 51–55
- Nicholls, A., Sharp, K. A., and Honig, B. (1991) *Proteins Struct. Funct. Genet.* 11, 281–296
- Petersen, E. F., Goddard, T. D., Huang, C. C., Couch, G. S., Greenblatt, D. M., Meng, E. C., and Ferrin, T. E. (2004) *J. Comput. Chem.* 25, 1605–1612
- Goda, N., Tenno, T., Takasu, H., Hiroaki, H., and Shirakawa, M. (2004) *Protein Sci.* 13, 652–658
- Hoeflich, K. P., and Ikura, M. (2002) *Cell* 108, 739–742
- Bhattacharya, S., Bunick, C. G., and Chazin, W. J. (2004) *Biochim. Biophys. Acta* 1742, 69–79
- Zhou, W., Qian, Y., Kunjilwar, K., Pfaffinger, P. J., and Choe, S. (2004) *Neuron* 41, 573–586
- Griffith, J. P., Kim, J. L., Kim, E. E., Sintchak, M. D., Thomson, J. A., Fitzgibbon, M. J., Fleming, M. A., Caron, P. R., Hsiao, K., and Navia, M. A. (1995) *Cell* 82, 507–522
- Kissinger, C. R., Parge, H. E., Knighton, D. R., Lewis, C. T., Pelletier, L. A., Tempczyk, A., Kalish, V. J., Tucker, K. D., Showalter, R. E., Moomaw, E. W., Gastinel, L. N., Habuka, N., Chen, X., Maldonado, F., Barker, J. E., Bacquet, R., and Villafranca, J. E. (1995) *Nature* 378, 641–644
- Yap, K. L., Ames, J. B., Swindells, M. B., and Ikura, M. (1999) *Proteins* 37,

Solution Structure of the NHE1-CHP1 Complex

- 499–507
49. Yap, K. L., Ames, J. B., Swindells, M. B., and Ikura, M. (2002) *Methods Mol. Biol.* 173, 317–324
50. Burgoyne, R. D., and Weiss, J. L. (2001) *Biochem. J.* 353, 1–12
51. Salerno, W. J., Seaver, S. M., Armstrong, B. R., and Radhakrishnan, I. (2004) *Nucleic Acids Res.* 32, W566–W568
52. Baumgartner, M., Patel, H., and Barber, D. L. (2004) *Am. J. Physiol.* 287, C844–C850
53. Denker, S. P., Huang, D. C., Orłowski, J., Furthmayr, H., and Barber, D. L. (2000) *Mol. Cell* 6, 1425–1436
54. Blom, N., Gammeltoft, S., and Brunak, S. (1999) *J. Mol. Biol.* 294, 1351–1362
55. Obenauer, J. C., Cantley, L. C., and Yaffe, M. B. (2003) *Nucleic Acids Res.* 31, 3635–3641
56. Ammar, Y. B., Takeda, S., Hisamitsu, T., Mori, H., and Wakabayashi, S. (2006) *EMBO J.* 25, 2315–2325



Cardiac Ischemia Activates Vascular Endothelial Cadherin Promoter in Both Preexisting Vascular Cells and Bone Marrow Cells Involved in Neovascularization

Naoko Kogata, Yuji Arai, James T. Pearson, Kazuaki Hashimoto, Kyoko Hidaka, Tatsuya Koyama, Satoshi Somekawa, Yoshikazu Nakaoka, Minetaro Ogawa, Ralf H. Adams, Masato Okada, Naoki Mochizuki

Abstract—Vascular endothelial cadherin (VE-cadherin) is expressed on vascular endothelial cells, which are involved in developmental vessel formation. However, it remains elusive how VE-cadherin-expressing cells function in postnatal neovascularization. To trace VE-cadherin-expressing cells, we developed mice expressing either green fluorescent protein or LacZ driven by VE-cadherin promoter using Cre-loxP system. Although VE-cadherin promoter is less active after birth than during embryogenesis in blood vessels, it is reactivated on cardiac ischemia. Both types of reporter-positive cells are found in the vasculature and in the infarcted myocardium. Those found in the vasculature were pre-existing endothelial cells and incorporated endothelial progenitor cells derived from extracardiac tissue. In addition to the vasculature, VE-cadherin promoter-activated cells were positive for CD45 in the bone marrow cells of the infarcted mice. VE-cadherin promoter-reactivated CD45-positive leukocytes were also found in the infarcted area. In addition, VE-cadherin promoter was activated in the bone marrow vessels of the infarcted mice. Collectively, our findings reveal a new ischemia-induced neovascularization mechanism involving VE-cadherin: the re-expressed VE-cadherin-mediated cell adhesion between cells may be involved not only in homing of bone marrow-derived cells to ischemic area but also mobilization from bone marrow. (*Circ Res.* 2006;98:897-904.)

Key Words: vasculogenesis ■ angiogenesis ■ hemangioblast ■ ischemia ■ CD45

Cell-based therapies have been aimed at neovascularization in ischemic diseases.¹ Recruitment of both angiogenic factor-producing hematopoietic cells and vasculature-constituting endothelial cells to the ischemic area contributes to neovascularization.² Endothelial progenitor cells (EPCs) and circulating bone marrow-derived EPCs (CEPCs) are incorporated into the nascent vessels.^{3,4} These cells have been suggested to originate from bone marrow. On the basis of this potential differentiation capability, bone marrow cell-based therapy has been attempted and proven to be effective for ischemic heart disease and peripheral artery disease.^{5,6} However, it is unclear how bone marrow-derived cells are recruited to the ischemic area.

Postnatal neovascularization includes angiogenesis and vasculogenesis. Both steps cooperatively work by involving the sprouting and branching of the pre-existing endothelial cells and recruiting EPCs in the vascular tree.⁷ Proangiogenic factors released from ischemic tissue and infiltrating cells, including vascular endothelial growth factor (VEGF), fibroblast growth factor, granulocyte macrophage colony-stimulating factor, and placental growth factor, mobilize

hematopoietic stem cells (HPCs) as well as EPCs to the infarcted area.^{8–10} Thus, HPCs and EPCs homing to the ischemic area are involved in angiogenesis and vasculogenesis in coordination with pre-existing vascular cells. Similar to adult neovascularization, embryonic vasculogenesis and angiogenesis are coordinated by both endothelial lineage cells and hematopoietic cells originating from hemangioblasts.

Several cell surface molecules, including CD133, VEGF receptor 2, vascular endothelial cadherin (VE-cadherin), and CD34, have been used to characterize the EPCs in the bone marrow and CEPCs in the peripheral blood.⁶ Although the cells purified by cell surface marker have been demonstrated to be recruited to the ischemic area when transferred for cell-based therapy, it is elusive how and what endogenous EPCs, CEPCs, and HPCs are mobilized to ischemic area for neovascularization in ischemic diseases.

VE-cadherin (Cadherin5, CD144), which belongs to cadherin super family, is expressed on cultured vascular endothelial cells and is essential for endothelial cell-cell interaction.¹¹ Whereas N-cadherin, another cadherin expressed on the endothelial cells, is thought to function in adherens

Original received April 20, 2005; revision received February 28, 2006; accepted March 8, 2006.

From the Departments of Structural Analysis (N.K., Y.N., T.K., S.S., N.M.), Bioscience (Y.A., K.H.), and Cardiac Physiology (J.T.P.); National Cardiovascular Center Research Institute, Osaka, Japan; the Department of Cell Differentiation, Institute for Molecular Embryology and Genetics (K.H., M.O.), Kumamoto University, Kumamoto, Japan; the Vascular Development Laboratory (R.H.A.), Cancer Research UK London Research Institute, United Kingdom; and the Department of Oncogene Research (M.O.), Institute for Microbial Disease, Osaka University, Japan.

Correspondence to Naoki Mochizuki, Department of Structural Analysis, National Cardiovascular Center Research Institute, 5-7-1 Fujishirodai, Suita, Osaka 565-8565, Japan. E-mail: nmochizu@ri.nccvc.go.jp

© 2006 American Heart Association, Inc.

Circulation Research is available at <http://circres.ahajournals.org>

DOI: 10.1161/01.RES.0000218193.51136.ad